Atmos. Chem. Phys. Discuss., https://doi.org/10.5194/acp-2018-75
Manuscript under review for journal Atmos. Chem. Phys.
Discussion started: 5 February 2018

Atmospheric Chemistry and Physics Discussions

Formation and characteristics of secondary aerosols in an industrialized environment during cold seasons

Yangzhou Wu[1], Xinlei Ge[1], Junfeng Wang[1], Yafei Shen[1], Zhaolian Ye[2], Shun Ge[3], Yun Wu[1], Huan Yu[1], Mindong Chen[1]

[1]Jiangsu Key Laboratory of Atmospheric Environment Monitoring and Pollution Control, Collaborative Innovation Center of Atmospheric Environment and Equipment Technology, School of Environmental Science and Engineering, Nanjing University of Information Science and Technology, Nanjing 210044, China
[2]College of Chemistry and Environmental Engineering, Jiangsu University of Technology, Changzhou 213001, China
[3]Nanjing Tianbo Environmental Technology Co., Ltd, Nanjing 210047, China

Correspondence to: Xinlei Ge (caxinra@163.com) and Mindong Chen (chenmdnuist@163.com)

Abstract. Secondary aerosols including inorganic and organic components often dominate the fine aerosol mass, it is thus important to elucidate the formation and characteristics of these species. In this work, we measured the submicron aerosols (PM_1) by using an Aerodyne high resolution soot-particle aerosol mass spectrometer in suburban Nanjing, China. The site was surrounded by industry plants, and the measurement was conducted during cold seasons (February-March 2015). We found that under such environment, the PM_1 was predominantly comprised of secondary species (on average 63.2% from ammonium sulfate and nitrate). Results show that moisture plays a key role to enhance both nitrate and sulfate formations. The moisture promotes the gas-particle partitioning and nocturnal heterogeneous production of nitrate, while transformation of SO_2 into sulfate directly in aqueous phase is more significant. The organic aerosol (OA) occupied ~1/4 of total PM_1 mass, and the

Atmos. Chem. Phys. Discuss., https://doi.org/10.5194/acp-2018-75
Manuscript under review for journal Atmos. Chem. Phys.
Discussion started: 5 February 2018

primary OA (POA) and secondary OA (SOA) contributions were almost equal. A specific industry-related OA was separated and a modified graphical method was introduced to describe the evolution of OA. Results further show that the most abundant OA factor, which is the one with highest oxidation degree, is also mainly driven by aqueous-phase processing, while the other two less oxygenated SOA factors are mainly governed by photochemical processing. Peak sizes of sulfate, nitrate and OA all shifted towards larger sizes with the increases of relative humidity, reflecting the effects of aqueous-phase processing too. Aqueous-phase driven secondary aerosols were found to be very important in enhancing the PM_1 pollution, while photochemical processed SOA was important to OA pollution, leading to a fresher OA at higher OA concentrations. We further demonstrated influences of the aqueous-phase processing and photochemical processing on formation of secondary aerosols by using two typical cases, respectively. This paper highlights the importance of aqueous-phase chemistry on sulfate and nitrate formations, and that different portions of SOA can be dominated by different mechanisms in an industrialized environment.

1. Introduction

Aerosol particles can significantly affect the earth's climate (e.g., Pöschl, 2005;Carslaw et al., 2010), air quality (e.g., Chan and Yao, 2008;Shen et al., 2017;Heal et al., 2012) and human health (e.g., Shiraiwa et al., 2017;Pope and Dockery, 2006;Hu et al., 2017), etc. However, such effects are highly uncertain, in a large part due to varying physicochemical properties of the particles, including sizes, compositions, and sources, etc. The secondary species, which often dominate the fine particle mass (e.g., Zhang et al., 2007;Huang et al., 2014), are particularly less understood. Formation of secondary components, including both inorganic and organic species, is very complex and dependent heavily upon atmospheric environments and meteorological conditions. For example, recent studies demonstrate that nitrate formation can be governed by multiple mechanisms in different seasons and locations of China (Ge et al., 2017a;Yang et al., 2017). For sulfate, it is well

known that the transformation of SO_2 into sulfate can occur in both gas-phase and aqueous-phase via reactions with multiple oxidants (Seinfeld and Pandis, 2016). Similarly, secondary organic aerosol (SOA) can be produced by both gas-phase and aqueous-phase (or multiphase/heterogeneous) reactions too (e.g., McNeill, 2015;Herrmann et al., 2015;Blando and Turpin, 2000;Lim et al., 2010). For examples, Zhang et al. (2018a) points out that both photochemical and aqueous-phase reactions can be important for the secondary organic carbon (SOC) in Shanghai during summertime, and aqueous-phase processing is more important to the SOC nighttime formation; Saffari et al. (2016) also shows the nighttime SOC formation in Los Angeles, while Ye et al. (2017b) shows that photochemical oxidation is important to the daytime SOC formation in Changzhou, China.

Due to a large variety of possible gaseous organic precursors, the formation pathways, yields and properties of SOA are complicated and much less clear compared with those of secondary inorganic aerosol (SIA). A large number of laboratory studies have been conducted to elucidate the characteristics of SOA produced by gas-phase oxidation (gasSOA) from certain precursors and the relevant mechanisms are continuously implemented into models (Ervens, 2015;Hallquist et al., 2009). Nevertheless, current models still cannot accurately reproduce the SOA mass or other properties, and the SOA produced in aqueous-phase (cloud/fog drops or aqueous aerosols) (aqSOA) is postulated to be a possible missing portion that can help reconcile the discrepancies (Ervens, 2015;Ervens et al., 2011;Heald et al., 2005). Correspondingly, studies regarding aqSOA formation have also made significant achievements recently (Herrmann et al., 2015;George et al., 2015a). For example, some volatile organic compounds, like isoprene (Liu et al., 2012), glyoxal and methylglyoxal (Lim et al., 2013), pyruvic acid (Carlton et al., 2006), amines (e.g., Ge et al., 2011b, a;De Haan et al., 2011), phenolic species (Yu et al., 2016;George et al., 2015b;Yu et al., 2014;Sun et al., 2010), etc., are found to be effective aqSOA precursors, and the aqSOA is significantly different from gasSOA in terms of product identities, volatility, hygroscopicity and optical properties (e.g., Lim et al.,

2013;Ervens et al., 2011).

As ambient conditions are more variable than the lab-controlled conditions, elucidation of secondary aerosol formation (including both SIA and SOA) and its influencing factors is more sophisticated. Traditional filter-based studies are limited in capturing the rapid evolution process, thus highly-time resolved measurements are necessary for a better interpretation of the secondary aerosol formation in ambient air (Wexler and Johnston, 2008). Recently, the Aerodyne Aerosol mass spectrometry (AMS) technique (Canagaratna et al., 2007) has emerged as a powerful tool, as it can quickly determine the concentrations, sizes and chemical compositions of fine aerosols (typically for submicron aerosols, PM_1). In combination with factor analysis (e.g., Zhang et al., 2011), it is able to resolve a few types of SOA, which may reflect different SOA formation mechanisms and/or evolution processes . For example, the effects of aqueous-phase and photochemical processing on the SOA formation in Beijing were discussed through analyses of multiple datasets (Xu et al., 2017a;Sun et al., 2016;Sun et al., 2013a). Formation of the aqSOA from AMS was also observed in other locations (e.g., Ge et al., 2012;Gilardoni et al., 2016;Li et al., 2013). Overall, these AMS results have greatly advanced our understanding on SOA (e.g., Jimenez et al., 2009;Li et al., 2017;Spracklen et al., 2011;Philip et al., 2014).

As is well known, Eastern China is frequently experiencing severe haze pollutions, and Yangtze River Delta (YRD) region is one of the heavily polluted regions (e.g., Hu et al., 2014). Previously, the AMS has been applied for online characterization of the fine aerosols in Nanjing (Shen et al., 2014;Zhang et al., 2015a;Zhang et al., 2016;Zhang et al., 2017;Wang et al., 2016b) and Hangzhou (Li et al., 2018) of this region. The offline AMS technique is also developed to analyze filter samples collected in Changzhou (Ye et al., 2017c;Ye et al., 2017a), and Yangzhou (Ge et al., 2017b) in the YRD region. In this study, we conducted a field campaign by using the most advanced AMS version, soot-particle aerosol mass spectrometer (SP-AMS)(Onasch et al., 2012) in suburban Nanjing during February - March 2015. The sampling site was near an industry zone, and indeed we reported earlier the

Atmos. Chem. Phys. Discuss., https://doi.org/10.5194/acp-2018-75
Manuscript under review for journal Atmos. Chem. Phys.
Discussion started: 5 February 2018

Atmospheric Chemistry and Physics Discussions

118 occurrence of fullerene soot, that was linked with industry emissions (Wang et al.,
119 2016c). In this work, we focused on analyzing the characteristics of secondary
120 aerosols in this special industrialized environment.
121
122 **2. Experimental Methods**
123 **2.1 Sampling site and instrumentation**
124 The sampling site and instrumentation was described in Wang et al. (2016c), thus
125 only a brief summary is provided here. The site resided in the Campus of Nanjing
126 University of Information Science and Technology (32°12′20.82″N, 118°42′25.46″E),
127 and the measurement period was February 20 to March 23, 2015. Particularly, the site
128 was located west/southwest of an industrial zone (mainly petrochemical, chemical,
129 iron and steelmaking, and power plants), close to the residential area and a few
130 arterial roads (within a radius of a few kilometers) (Fig. 1). Therefore, the site was
131 probably influenced by the mixed emissions from industry, traffic and cooking, etc.
132 Our main instrument was SP-AMS, which was carefully tuned and strictly
133 calibrated for both mass quantification and sizes following the standard protocols
134 (details in Wang et al. (2016c)). The SP-AMS was operated with a dual-vaporizer
135 setup (with both laser and tungsten vaporizers), and the laser was switched alternately,
136 thus we were able to determine the chemical compositions and size distributions of
137 both non-refractory species (ammonium, sulfate, nitrate, chloride and organics) and
138 refractory black carbon (*r*BC). Concentrations of $PM_{2.5}$ and gaseous species (CO,
139 NO_2, SO_2 and O_3) were acquired from the nearest environmental monitoring site. The
140 meteorological parameters, including air temperature (T), relative humidity (RH),
141 wind speed (WS), wind direction (WD), solar radiation and visibility were provided
142 by a meteorological station ~50m away from our site.
143
144 **2.2. Data analyses**
145 The SP-AMS data were processed by using the Igor Pro-based (Wavemetrics)
146 standard ToF-AMS analysis toolkit SQUIRREL version 1.59D and PIKA version

1.19D (Sueper, 2015). All mass concentrations were calculated from the high resolution fitting of V-mode data (a mode sensitive to mass changes). The *r*BC concentrations were from V-mode with both laser and tungsten vaporizers on, while concentrations of other non-refractory species were from V-mode with the tungsten vaporizer only. The calibrated relative ionization efficiencies (RIEs) were used to account for the different instrument responses to different species. Also, the composition-dependent collection efficiencies (CE) (Middlebrook et al., 2012) were applied to consider the particle loss due to incomplete transmission, and particle bouncing from the tungsten heater. All these data were averaged into hourly data when comparing with the meteorological parameters or gaseous species. The data reported are at local time (Beijing time).

The high chemical resolution of SP-AMS allows us to separate different ions and derive the elemental ratios of OA including oxygen-to-carbon (O/C), hydrogen-to-carbon (H/C), nitrogen-to-carbon (N/C) ratios, and organic mass to organic carbon (OM/OC) ratios. The method proposed by Canagaratna et al. (2015)(referred to as I-A method) was used here unless otherwise stated. The I-A method is an update of the Aiken-ambient (A-A) method (Aiken et al., 2008), which improved the calculation of O/C and H/C ratios. Results from I-A method correlated very well with those from A-A method (Fig. S1 in the supplement), but increased the O/C, H/C and OM/OC on average by 27%, 9% and 8.5%, respectively.

Positive matrix factorization (PMF) (Paatero and Tapper, 1994) and the PMF Evaluation Toolkit version 2.08D (Ulbrich et al., 2009) were applied on the high resolution mass spectra of OA acquired under W-mode (a mode with high mass resolution, ~4000 in this work) with the dual-vaporizer setting. Six OA factors were identified, including three primary factors relevant with traffic (HOA), cooking (HOA), industry (IOA), and three secondary OA factors which are a semi-volatile oxygenated OA (SVOOA), a low-volatility OA (LVOOA) and a local secondary OA (LSOA). Procedures of the PMF analyses, justifications and diagnostics of the optimal PMF solution, and the high resolution mass spectra (HRMS) of the factors

were presented in details in Wang et al. (2016c). In this work, we focused on analyzing the features and behaviors of these OA factors, in particular the unique primary IOA and three SOA factors.

3. Results and discussion

3.1. Overview of the PM_1 characteristics

Figure 2 shows the time series of meteorological parameters (T, RH, solar radiation, WS, WD), concentrations of gaseous species (NO_2, O_3, SO_2 and CO), fractional contributions of different PM_1 components (sulfate, nitrate, chloride, ammonium, organics and *r*BC) to the total PM_1, and different OA factors (HOA, COA, IOA, LSOA, SVOOA and LVOOA) to the total OA. The weather was overall humid during the sampling period with an average RH of ~70%. There were also a few precipitation events, for example, intermittently on February 28-March 1 and March 17-19, unfortunately the precipitation data were not recorded due to malfunction of the meteorological meter. The wind was not very strong (average 1.4 m/s) and mostly blew from east/northeast directions (Fig. S2). As a number of industrial plants located east/northeast of our site, the measured PM was expected to be influenced by industrial emissions. The campaign acrossed the later winter and early spring, thus the temperature varied significantly from 0ºC to 21ºC with a mean of 8.5ºC. The later days (March 13-23) were much warmer than the earlier days (12.5ºC vs. 6.0ºC).

The PM_1 concentrations varied dynamically from 8.4 to 180.5 μg/m^3, with an average of 46.3 μg/m^3, and was dominated by inorganic components (68.4%) (Fig. 3a). Such mass contribution from inorganic species in PM_1 was higher than most AMS measurements in both urban and rural sites of China (Li et al., 2017) and other countries (Jimenez et al., 2009), likely reflecting the SO_2 and NO_x emissions enhanced by industry at this specific location. *r*BC contributed 6.1% of PM_1 mass. Organics, on average, was still the most abundant component but only took up 25.5% of PM_1 mass. The average contribution from POA (=HOA+COA+IOA) (52%) was almost equal to that of SOA (=LSOA+SVOOA+LVOOA) (48%) (Fig. 3b). Taking

Atmos. Chem. Phys. Discuss., https://doi.org/10.5194/acp-2018-75
Manuscript under review for journal Atmos. Chem. Phys.
Discussion started: 5 February 2018

together, the secondary components (SIA and SOA) occupied ~82% of the PM_1 mass. This fraction is higher than those observed in $PM_{2.5}$ in a few Chinese megacities during heavy haze periods (30-77%) (Huang et al., 2014). It points out that even in an environment that is expected to have significant primary emissions, secondary species still plays a major role to the aerosol pollution, indicating that the precursors (SO_2, NO_2 and SOA precursors) can be efficiently oxidized in such atmosphere.

The average size distributions of different species are shown in Fig. 3c. The major inorganic species all peaked in the accumulation mode (~650 nm D_{va}), representing their behaviors as secondary species. Relatively, the organics had a wider size distribution and peaked at a smaller size (~550 nm D_{va}), indicating it was a mixture of both primary and secondary species. Size distribution of *r*BC was significantly different from other components (peak D_{va} of 250-500 nm), as it was predominantly originated from primary sources.

We also compared the mass concentrations of PM_1 determined by SP-AMS with the $PM_{2.5}$ concentrations from the nearest monitoring station in Fig. 3d. Generally, they correlated well with each other (r^2=0.70), and the PM_1 on average occupied ~83% of $PM_{2.5}$. This $PM_1/PM_{2.5}$ fraction is higher than those previously observed in urban Nanjing, for example, 54% during springtime (Wang et al., 2016b) and 63% during wintertime (Zhang et al., 2016), showing a more significant contribution from small particles in an environment affected by industry than the average urban case.

3.2 Sulfate and nitrate formations

As shown in Fig. 3a, sulfate and nitrate were abundant in PM_1. By assuming they were associated with ammonium, $(NH_4)_2SO4$ and NH_4NO_3 together would dominate the PM_1 mass (63.2%). In Fig. 4, we presented the variations of sulfate and nitrate concentrations as functions of RH and the odd oxygen (O_x=O_3+NO_2) over the entire sampling period. Typically, RH is an indicator of atmospheric moisture and is relevant with aqueous-phase/heterogeneous reactions (Tie et al., 2017), while O_x can be used to represent photochemical activities (Herndon et al., 2008). From Fig. 4a, both

sulfate and nitrate concentrations increased substantially with the increase of RH, especially at RH>65%. Note the decreases at RH>90% were probably due to the scavenging effects of precipitation (we have no exact precipitation data so cannot accurately eliminate such influences). On the other hand, sulfate and nitrate both presented no clear increases with the increase of O_x (Fig. 4b). The image plots which describe the dependences of nitrate (Fig. 4c) and sulfate (Fig. 4d) on RH and O_x, also showed that high mass concentrations of sulfate and nitrate appeared mainly in the regimes with RH>65%, but distributed evenly across the changes of O_x. These results highlight a more significant role of moisture in enhancing the formation of both sulfate and nitrate than that of photochemical processing. Similar effects of RH on sulfate and nitrate were also observed in urban Jinan, China (Wang et al., 2012).

As is well known, ammonium nitrate is semi-volatile and water can enhance its thermodynamic gas-particle partitioning and dissolution in the particle phase. Our results clearly reveal that this "thermodynamically-driven" mechanism (Ge et al., 2017a) is critical in governing the nitrate variations in Nanjing. During nighttime, the heterogeneous hydrolysis of N_2O_5 can also contribute to nitrate production. It is worth to mention that the nitrate formation mechanisms may vary greatly, for example, during wintertime in Beijing, photochemical production of nitrate is more evident (Sun et al., 2013b). On the other hand, ammonium sulfate is non-volatile and thermodynamic partitioning affects its concentrations in a much lesser extent, however water as a reaction medium, may facilitate the oxidation of SO_2 into sulfate (Seinfeld and Pandis, 2016). In a word, although high RH can promote formations of both nitrate and sulfate, the underlying detailed processes are different.

To further investigate the sulfate and nitrate formation mechanisms, we calculated the sulfur oxidation ratio (SOR = $n{SO_4}^{2-}/(n{SO_4}^{2-}+n{SO_2})$) and nitrogen oxidation ratio (NOR = $n{NO_3}^{-}/(n{NO_3}^{-}+n{NO_2})$). Here $n{SO_4}^{2-}$, $n{NO_3}^{-}$, $n{SO_2}$ and $n{NO_2}$ are the molar concentrations of particle-phase sulfate, nitrate, gaseous sulfur dioxide and nitrogen dioxide, respectively. Note since there are multiple gas-phase forms of nitrogen oxides (NO, N_2O_3, N_2O_4, N_2O_5, etc) rather than only NO_2, the NOR actually should

Atmos. Chem. Phys. Discuss., https://doi.org/10.5194/acp-2018-75
Manuscript under review for journal Atmos. Chem. Phys.
Discussion started: 5 February 2018

Atmospheric Chemistry and Physics Discussions

be smaller than those calculated here. The dependences of NOR and SOR on RH are shown in Figs. 5a and 5b. The NOR was elevated from 0.09-0.13 (average: 0.12) at RH<65% to 0.19-0.22 (average: 0.21) at RH>65%, yet there was no significant enhancement when RH increased from 65% to 95%. Different from NOR, SOR increased nearly linearly with RH from 0.07 at RH=35% to 0.50 at RH=95% by a large factor of 7.4. The mean SOR under RH>80% was 0.46, much higher than 0.23 observed in wintertime Beijing at RH=80-90% (Sun et al., 2013a), likely indicating a stronger aqueous-phase SO_2 oxidation ability in Nanjing. The comparison between NOR and SOR shown here demonstrates that moisture in fact plays a more important role for sulfate formation than it does for nitrate. These results also suggest that by considering increases of particle-phase sulfate and nitrate alone, may not well reflect the RH effects, as nitrate concentrations actually increased more rapidly than that of sulfate with the increase of RH: From RH of 40 to 90%, nitrate increased from 5.1 to 16.6 $\mu g/m^3$, while sulfate increased from 6.8 to 13.9 $\mu g/m^3$. This result likely suggests that a significant portion of nitrate is due to gas-to-particle conversion rather than direct production in aqueous-phase. Previous studies show that the presence of NO_2 actually can enhance aqueous-phase sulfate formation under humid/foggy/cloudy conditions in Nanjing (Xie et al., 2015) and Beijing (Cheng et al., 2016;Wang et al., 2016a), though the significance of this mechanism is heavily dependent upon the RH conditions (Liu et al., 2017;Guo et al., 2017;Zhang et al., 2018b).

Correspondingly, Figures 5c and 5d illustrate the variations of NOR and SOR as a function of O_x ceontrations. NOR showed no obvious dependence on O_x, suggesting that photochemical production of nitrate is not significant. While SOR displayed an overall decreasing trend with the increase of O_x concentrations. As high RH was associated with low solar radiation (Fig. 1) and low O_x concentrations (Figs. 4a and 4b), this result, on the other hand, underscores the dominance of aqueous-phase processing over photochemical processing for sulfate production. In addition, both NOR and SOR did not vary significantly with changes of temperatures (Fig. S3b), again supporting that they were not significantly influenced by photochemical

Atmos. Chem. Phys. Discuss., https://doi.org/10.5194/acp-2018-75
Manuscript under review for journal Atmos. Chem. Phys.
Discussion started: 5 February 2018

processes. Moreover, the aqueous-phase sulfate production is actually insignificant during springtime in urban Nanjing when the temperature is warmer and the air is drier, as revealed in our previous study (Wang et al., 2016b). Therefore, the findings point out that aerosol sulfate chemistry can be very different under different seasons in the same region. In addition, a measurement study conducted almost in the same period as this study in Beijing (Zhang et al., 2018c) reported the dominance of aqueous-phase production of sulfate, while nitrate was mainly produced by photochemical and heterogeneous reactions. These results indicate that the formation mechanisms of sulfate and nitrate can be different at different locations in the same season.

3.3 Secondary organic aerosol (SOA) formation

3.3.1 Industry-related OA

A specific OA factor – industry-related OA (IOA) was resolved by the PMF analysis in this study. This factor on average occupied ~1/6 of the total OA mass, equivalent to ~1.9 μg/m^3. It was different from those from traffic and cooking, as their time series were significantly different (r^2 of 0.03 for HOA *vs.* IOA, and r^2 of 0.01 for COA *vs.* IOA). Also, across the sampling period, its temporal variations were relatively smaller than those of HOA and COA, indicating it was a persistent source in this region.

The ion-specified HRMS by six ion families is presented in Fig. 6. The IOA O/C ratio (0.44 from I-A method, and 0.33 from A-A method) was relatively high as a POA factor, but was still within a reasonable range. The most abundant ion category in IOA was the chemically-reduced hydrocarbon ions (46%, Fig. 6), but it also had a high contribution from oxygenated ions (especially CO_2^+ and $C_2H_3O^+$). Previously, an industry-related OA factor from the PMF analyses of both online measurement data (El Haddad et al., 2013) and offline $PM_{2.5}$ samples in Marseille (France) (Bozzetti et al., 2017) was reported. Similar to our IOA, the factor resolved by Bozzetti et al. (2017) had a high CO_2^+ peak (~10% of total) and a O/C ratio of 0.33. This

321 industry-related OA factor in Marseille was attributed to contributions from coke,
322 steel and petrochemical facilities, which is also very similar to the industry zone
323 adjacent to our site.

324 It should be noted that, the IOA MS had also relatively higher fractions $C_2H_4O_2^+$
325 (*m/z* 60) and $C_3H_5O_2^+$ (*m/z* 73) than other factors did. These two ions are often used as
326 biomass burning OA tracers as they can be produced by levoglucosan (Aiken et al.,
327 2010). However, a recent study (Yan et al., 2018) showed that coal combustion could
328 be a significant source of levoglucosan in China. The AMS mass spectrum of peat
329 burning OA was also found to contain appreciable *m/z* 60 and *m/z* 73 signals (Lin et
330 al., 2017). Considering that the winds during this campaign were mostly blew from
331 the industry zone with coal (power plants and steel works) and oil burning (petroleum
332 industry) (Fig. S2), and the open biomass burning was banned by the government in
333 this region, the $C_2H_4O_2^+$ and $C_3H_5O_2^+$ signals were likely associated with industry
334 emissions. Of course, more studies are required to further elaborate the characteristics
335 of IOA, including molecular characterization of specific industry-related organic
336 tracer compounds and measurement of the heavy metals which are typically
337 associated with industry emissions.

338 **3.3.2 A modified method to separate SOA from POA**

339 Previously, Ng et al. (2010) proposed to use a triangle plot of *f*44 (ratio of *m/z* 44
340 to total signal of the OA factor) versus *f*43 (ratio of *m/z* 43 to total signal of the OA
341 factor) as a diagnostic to describe different OA factors. Ambient OA in this *f*44:*f*43
342 space typically converges to the upper left corner with the ageing of OA. This is
343 because *f*44 (mainly CO_2^+) is representative of highly oxygenated carboxylic acids
344 while *f*43 (mainly $C_2H_3O^+$) is mainly produced from non-carboxylic oxygenated
345 species. This plot is presented in Fig. 7b. For this dataset, separation of the factors
346 (especially HOA, IOA, LSOA and SVOOA) was not very well by using this method.
347 Chhabra et al. (2011) also shows that the movement paths of different SOA
348 components in the *f*44:*f*43 space depend on the precursors. Generally speaking, *f*44
349 and *f*43 use only two fragments, they may sometimes not well represent the general

Atmos. Chem. Phys. Discuss., https://doi.org/10.5194/acp-2018-75
Manuscript under review for journal Atmos. Chem. Phys.
Discussion started: 5 February 2018

Atmospheric Chemistry and Physics Discussions

properties of OA. In addition, *m/z* 44 and *m/z* 43 may be significantly influenced by other ions, such as $C_3H_7^+$ on *m/z* 43 and $C_2H_4O^+$/$C_2H_6N^+$ on *m/z* 44.

Heringa et al. (2012) proposed another method to discriminate different OA factors. Following this method, we first re-sorted the HRMS according to the number of carbon (C_1-C_7) and oxygenation state (C_x, C_xO_1, $C_xO_{>1}$) of each fragment ion. Each HRMS was grouped into 21 clusters and displayed in Fig. 7a. Then, we placed our six PMF-resolved OA factors into the two-dimensional space of C_2/C_2O_1 vs. $C_3O_1/C_3O_{>1}$ as suggested by Heringa et al. (2012). As shown in Fig. 7c, the HOA and COA fell far from SVOOA and LVOOA, while IOA and LSOA were still very close to each other. Since the method in fact still uses only a few ions, it is likely better to represent the average properties of OA by making use of the chemical information from more ions. For this purpose, the six OA factors were projected into the fC_xO_y/fC_xR (or $fC_xRO_{>1}/fC_xRO_1$) vs. $fC_{x\geq3}R/fC_{x\leq2}R$ spaces (Figs. 7d and 7e). Here fC_xO_y/fC_xR is the ratio of all oxygen-containing ions (C_xO_y) to all oxygen-free ions (C_xR), $fC_xRO_{>1}/fC_xRO_1$ is the ratio of ions with more than one oxygen atoms to those with only one oxygen atom, and $fC_{x\geq3}R/fC_{x\leq2}R$ is the ratio of hydrocarbon ions at $x\geq3$ to those at $x\leq2$. As shown in Fig. 7a, with increase of oxidation degrees (O/C) of the OA factors, the contribution from C_x groups at $x\leq2$ gradually increased, while contribution from hydrocarbon ions (C_xR) with $x\geq3$ decreased. The small ion fragments also contained more oxygenated ions, likely reflecting the abundance of small organic acids. This trend suggests that the ageing of OA proceeds with fragmentation of large molecules, and a $fC_{x\geq3}R/fC_{x\leq2}R$ ratio can reflect such reaction pathway. On the other hand, the ageing of OA often involves the oxidation of hydrocarbon species, thus the fC_xO_y/fC_xR ratio or $fC_xRO_{>1}/fC_xRO_1$ ratio may indicate the oxidation of OA. In both Fig. 7d and Fig. 7e, the SOA factors locate in the upper left region, and can be better separated from the POA factors than that by using the *f*44:*f*43 space. In particular, the different OA factors approached to the upper left corner in a consecutive order which was consistent with their O/C ratios, and the movement trajectory was also close to a straight line (y=1.89-0.39x, r^2=0.85). This

Atmos. Chem. Phys. Discuss., https://doi.org/10.5194/acp-2018-75
Manuscript under review for journal Atmos. Chem. Phys.
Discussion started: 5 February 2018

result suggests that the (fC_xO_y/fC_xR):($fC_{x\geq3}R/C_{x\leq2}R$) space is probably a more effective metric to separate different OA factors and demonstrate the evolution of OA.

It should be mentioned that Heald et al. (2010) proposed to use a Van Krevelen diagram (H/C versus O/C) to describe the OA ageing, as shown in Fig. S4 for this dataset. Compared to the *f*44:*f*43 space (Ng et al., 2010), this method uses the bulk composition of OA. Our modified method proposed here seems to balance the level of chemical information, not only dependent upon a couple of specific ions, but also not rely on the general properties without incorporating detailed ion compositions. Of course, more tests by using more ambient datasets are strongly needed in the future to verify this graphical method.

3.3.3 Effects of aqueous-phase and photochemical processing

In this study, we identified three SOA factors (LSOA, SVOOA and LVOOA), which together occupied nearly half of OA mass. We plotted the mass concentrations and fractional contributions of the three SOA factors against RH and O_x, to investigate the effects of aqueous-phase and photochemical processing on their formations (Fig. 8). Generally, the concentrations of LVOOA presented an increasing trend with RH, and its mass fraction increased more obviously from only 4% at RH<40% to 32% at RH>90%, while those of LSOA and SVOOA showed no such trends. This result demonstrates the importance of aqueous-phase processing on LVOOA formation. On the contrary, both mass loadings and fractions of LSOA and SVOOA increased obviously with the increase of O_x, while those of LVOOA decreased significantly from 46% at O_x<50 μg/m^3 to 9% at O_x>140 μg/m^3. Such relationships reveal that photochemical processing promotes the LSOA and SVOOA formations, but contributes negligibly or even hinders the formation of LVOOA. Note the LVOOA had the highest O/C ratio (0.74) among the three SOA factors. This is consistent with the facts that aqSOA typically has a high oxidation level as discovered by a number of lab studies (e.g., Herrmann et al., 2015), and the aqSOA products have low volatility in general and contribute significantly to LVOOA (Ervens et al., 2011). Our results clearly demonstrate the close link between LVOOA and aqSOA. The LSOA and

Atmos. Chem. Phys. Discuss., https://doi.org/10.5194/acp-2018-75
Manuscript under review for journal Atmos. Chem. Phys.
Discussion started: 5 February 2018

SVOOA were relatively fresher with O/C ratios of 0.44 and 0.66, respectively. Our results suggest that the relatively fresh SOA is closely associated with gasSOA (SOA produced from gas-phase photochemical reactions). These findings are in good agreement with those observed in urban Beijing (Xu et al., 2017a), likely representing the general characteristics of the AMS-resolved OOA factors.

For reference, we also checked the variations of POA factors (HOA, COA and IOA) against RH and O_x (Fig. S5). Results show that both concentrations and fractions of the POA factors overall had no clear responses to either RH or O_x increases, which are in accordance with their behaviors as POA – they were emitted directly into the air thus were not expected to be influenced by both aqueous-phase or photochemical processing. One exception was that COA concentrations seemed to increase with O_x, which was likely a coincidence as the lunchtime was exactly noon/early afternoon with strong photochemical activities.

To further investigate the influences of aqueous-phase and photochemical processing on the oxidation levels of SOA (O/C$_{SOA}$), we calculated the O/C$_{SOA}$ based on the method proposed by Xu et al. (2017b). It represents the combined O/C ratio of the summed LSOA, SVOOA and LVOOA. The changes of O/C$_{SOA}$ and O/C$_{OA}$ (the O/C ratios of total OA) versus RH and O_x were shown in Figs. 8e and 8f. The O/C$_{OA}$ showed no clear dependences on both RH and O_x, probably due to the mixing effects of POA. However, the O/C$_{SOA}$ tended to be larger at higher RH (especially at RH>60%), indicating the contribution of more oxygenated aqSOA; while the O/C$_{SOA}$ clearly decreased with increase of O_x concentrations (from 0.71 at O_x<50 μg/m^3 to 0.57 at O_x>140 μg/m^3), as more photochemical SOA with lower O/C ratios were generated.

The combined effects of RH and O_x were further illustrated in Fig. 9. High SVOOA and LSOA concentrations appeared in the regimes with high O_x concentrations (Figs. 9a and 9b) and high fractions of these two factors also tended to be accompanied more significantly with low RH conditions (Figs. 9d and 9e). Differently, both high concentrations and high fractions of LVOOA located in the

upper left corner characterized by high RH and low O_x conditions (Figs. 9c and 9f), again supporting the importance of aqueous-phase processing on LVOOA production.

Furthermore, it is known that different formation pathways have different impacts on the size distributions of fine aerosols. Secondary species from gas-phase photochemical reactions typically condense on smaller particles (condensation mode), while particles from aqueous-phase reactions in clouds/fogs or wet aerosols are larger (droplet mode) (Ervens et al., 2011;Kerminen and Wexler, 1995;Meng and Seinfeld, 1994). Enhancements of particle sizes were indeed observed when aqueous-phase reactions occurred (Gilardoni et al., 2016;Ge et al., 2012). In this regard, we investigated the average size distributions of OA, sulfate and nitrate at different RH levels (Fig. 10). Obviously, the peak sizes of OA, sulfate and nitrate all shifted towards larger sizes with the increase of RH. The OA size distribution peaked at 268 nm D_{va} (vacuum aerodynamic diameter) at RH<40%, and increased substantially to 694 nm D_{va} at RH of 88-92%. Because increase of RH did not elevate the three POA (Fig. S5), LSOA and SVOOA factors (Figs. 8a and 8b), the growth of OA sizes can be attributed mostly to the formation of LVOOA, namely aqSOA. The peak D_{va} of sulfate increased from 418 nm (RH<40%) to 730 nm (RH=88-92%), and that of nitrate increased even more significantly – from 233 nm (RH<40%) to 694 nm (RH=88-92%). Small drops of the peak D_{va} occurring at RH>92% for all three species, were probably due to the scavenging effects of precipitation. Overall, the enhancements of peak sizes of OA, sulfate and nitrate by RH provide another evidence supporting the importance of aqueous-phase processing on secondary aerosol formation in this study.

3.4. Influences of secondary aerosol formation on PM_1 pollution

3.4.1 Mass contributions at different pollution levels

We have demonstrated that moisture plays important roles to the formations of sulfate, nitrate and LVOOA, while photochemical processing is important for LSOA and SVOOA productions. Here we investigated contributions of these secondary

components at different levels of PM_1 and OA pollutions. As shown in Fig. 11a, mass fractions of nitrate increased from 16.5% during clean periods (PM_1<10 μg/m^3) to ~26-27 % during polluted periods (PM_1>60 μg/m^3) (there was a small drop from 27.1% at PM_1 of 60-70 μg/m^3 to 25.9% at PM_1>70 μg/m^3). Variations of sulfate contribution were relatively small from 25.2% at PM_1<10 μg/m^3 to 21.1% at PM_1>60 μg/m^3. We also illustrated the mean RH and O_x concentrations at different PM_1 levels in Fig. 11a. With the aggravation of PM_1 pollution, RH also significantly increased (from 57% to 83%), but O_x concentrations varied very little within a range of 82.3 - 90.3 μg/m^3. This result shows the importance of moisture to haze pollution as it promotes the formations of nitrate and sulfate. In fact, both NOR and SOR values increased with the increase of PM_1 concentrations (Fig. S3a). As we showed earlier, nitrate concentrations increased more quickly with RH than that of sulfate, thus its fractions increased significantly, while the sulfate concentrations increased but its relative contributions decreased slightly. The faster increase of nitrate concentrations than sulfate during heavy pollution was also observed in Nanjing during 2014 (Wu et al., 2017), Nanjing (Zhang et al., 2015b) and Lin'an (Shen et al., 2015) during 2013 January in the YRD region. This is different from that in North China Plain, where sulfate often plays a more significant role in heavy haze formation.

For organics, the contributions continuously decreased from 32.3% at PM_1<10 μg/m^3 to 23.6% at PM_1>70 μg/m^3 (Fig. 11a). This result indicates that although high RH could enhance the production of a portion of SOA (namely the LVOOA), overall, the OA pollution was not governed by RH effects. Therefore, we calculated the mass fractions of different OA factors to total OA at different OA levels in Fig. 11b. Clearly, the LVOOA contributions changed from 25.2-29.0% at OA<10 μg/m^3 down to only 10.4% at OA>30 μg/m^3, while the sum of LSOA and SVOOA increased substantially from 12.1% at OA<5 μg/m^3 to 45.1% at OA>30 μg/m^3. This result shows that photochemical processing was more important than the aqueous-phase processing in exacerbating the OA pollution. Correspondingly, we found that the RH did not vary significantly as a function of OA concentrations (within 70-80%), while O_x

concentrations increased obviously from 77.6 μg/m^3 at OA<5 μg/m^3 to 115.7 μg/m^3 at OA>30 μg/m^3. This is somewhat opposite to the case of PM_1, and partially explains the decrease of OA contributions to the heavy PM_1 pollutions. In addition, the total POA mass fractions decreased from 62.7% at OA<5 μg/m^3 to 44.5% at OA>30 μg/m^3. This is different from that found during springtime in urban Nanjing (Wang et al., 2016b), where the heavier OA pollution periods were accompanied by elevated POA contributions.

Moreover, we calculated $fCO_2^+/fC_2H_3O^+$ and Y/X (Y=fC_xO_y/fC_xR, X=$fC_{x\geqslant3}R/fC_{x\leqslant2}R$) against OA concentrations in Fig. 11c. The $fCO_2^+/fC_2H_3O^+$ modified the *f*44/*f*43 index (Ng et al., 2010) as it eliminates influences from other ions on *m/z* 44 and *m/z* 43. Both indexes decreased with OA concentrations, showing that the reduction of highly oxygenated LVOOA contributions and increase of moderately oxidized LSOA and SVOOA contributions compensated the decrease of fresh POA contributions. Correspondingly, $fC_4H_9^+$ and $fC_{x\geqslant3}R/fC_{x\leqslant2}R$ increased with the increase of OA concentrations. As $C_4H_9^+$ (*m/z* 57) is often used a POA tracer, and $fC_{x\geqslant3}R/fC_{x\leqslant2}R$ also reflects the abundance of chemically reduced hydrocarbon ions (Section 3.3.2), this result again suggests the OA overall became less oxygenated when its pollution became heavier. All results underscore that the relatively fresh and photo-formed SOA (LSOA and SVOOA) plays dominant roles to the OA pollution in this industrialized environment.

In addition, we checked the variations of mass fractions of different components at different wind speeds (WS) and wind directions (WD) (Fig. S6). Generally, the changes were not dramatic, consistent with those of RH (67%-79%) and O_x (79-95 μg/m^3), which did not present clear increasing or decreasing trends against WS and WD as well. Such results indicate that the influences of secondary aerosol species seemed to be not affected significantly by the different air masses in this location.

3.4.2 Case studies

We investigated influences of secondary aerosol formation in two specific cases. The first case was from 3:30pm March 1 to 3:30 pm March 2 (marked in Fig. 2).

524 During this episode, the mean PM_1 concentrations was 48.9μg/m^3, and the summed
525 mass contributions from $(NH_4)_2SO_4$, NH_4NO_3 and LVOOA to PM_1 was 74.4%, both
526 higher than their corresponding campaign-average values (46.3μg/m^3 and 68.6%, Fig.
527 3a). This episode was characterized by significant productions of sulfate, nitrate and
528 LVOOA (SNL). The total PM_1 concentrations were very closely linked with the SNL
529 formation (Fig. 12b) especially during later afternoon and nighttime. Correspondingly,
530 the enhancement of SNL almost linearly responded to the increase of RH (r=0.96),
531 but oppositely correlated with that of O_x (r=-0.86). High RH during nighttime were
532 associated with high SNL concentrations, while high O_x concentrations during
533 noon/early afternoon were accompanied by low SNL concentrations.

534 Another case was characterized by relatively significant photochemical formation
535 of SOA, especially the LSOA. This episode lasted from the early evening of March 12
536 till early morning of March 16 (marked in Fig. 2). In fact, high LSOA concentrations
537 mainly occurred in this period, which was on average 4.8 μg/m^3, much higher than its
538 average value of 0.38 μg/m^3 during other periods. This is actually one reason it was
539 defined as LSOA since it was most likely a specific and localized event. We found it
540 was mainly driven by photochemical processing (Section 3.3.3), but unable to identify
541 the precursors whose emissions were particularly enhanced during this episode and
542 led to the LSOA formation due to measurement limitations. During this period, the
543 mean OA concentration was 18.3 μg/m^3 (Fig. 13a), much higher than its
544 campaign-average value of 11.8 μg/m^3; mass fraction of LSOA and SVOOA (LSS)
545 together was 43.6% (Fig. 13a), also higher than the campaign average of 26.4%.
546 Similar as those in Fig. 8, we observed the enhancements of LSS mass concentrations
547 and fractions at high O_x concentrations but reductions at high RH conditions (Fig. S7).
548 More clearly, from noontime of March 15 to early morning of March 16, the LSS
549 mass concentrations correlated positively very well with O_x (r=0.91) but meanwhile
550 linearly decreased with RH (r=-0.90) (Figs. 13b and 13c). Contrary to the first case
551 (Fig. 12), high O_x concentrations during noon/afternoon associated with high LSS
552 concentrations, while high RH during nighttime associated with low LSS

concentrations. These two cases are two typical examples demonstrating especially the aqueous-phase nighttime formation of SNL and the daytime photo-formation of LSS, respectively.

4. Conclusions

This work presents the field measurement results focusing on the formation and characteristics of secondary inorganic (mainly sulfate, nitrate) and organic species, by using the SP-AMS in suburban Nanjing during February – March, 2015. The site was surrounded by a large number of industrial plants. Nevertheless, under this industrialized environment, the PM_1 was mainly comprised of secondary aerosol components (75.4%), including 63.2% from ammonium sulfate and nitrate, and 12.2% from SOA. This finding indicates that the gas-phase precursors such as SO_2, NO_2 and volatile organic compounds can be effectively transformed into particle-phase species. Furthermore, moisture was found to play a major role in enhancing productions of sulfate, nitrate and the highly oxygenated portion of SOA (LVOOA, 45% of SOA), yet the detailed mechanisms were different. The moisture likely affected nitrate by enhancing its thermodynamic gas-particle partitioning and nocturnal heterogeneous production, while direct productions of sulfate and LVOOA in aqueous phase were more significant. In addition, the peak sizes of sulfate, nitrate and OA all shifted towards larger sizes with the increases of relative humidity, reflecting the effects of aqueous-phase processing too. On the other hand, the other two less oxygenated SOA factors (LSOA and SVOOA, together 55% of SOA) were mainly driven by photochemical processing.

Overall, the moisture-driven nitrate and sulfate productions were important to aggravate the PM_1 pollution. The photo-chemically formed SOA was more important than the aqueous-phase SOA to OA pollution. The influences of these two formation pathways were demonstrated very clearly in two typical episodes. In addition, in this study we also provided two new findings. First, we separated a specific industry-related OA factor. Secondly, we proposed a modified graphical method to

describe the evolution of OA. Both of them should be investigated and verified in the future with other AMS datasets. In summary, this work highlights that aqueous-phase chemistry is very important for sulfate and nitrate productions in an industrialized environment during cold seasons. We also show that the highly oxygenated SOA is very likely linked with aqueous-phase processing while the less oxygenated ones are associated with photochemical processing.

5. Data availability

The observational data in this study are available from the authors upon request (caxinra@163.com).

Acknowledgements

This work was financially supported by the Natural Science Foundation of China (Grant Nos. 91544220, 21577065 and 21777073), the Jiangsu Natural Science Foundation (BK20150042), the Jiangsu Provincial Specially-Appointed Professors Foundation, and the startup foundation for introducing talent of NUIST (2014r064). The authors also acknowledge the helps from Yanan He, Ling Li, Hui Chen and Yanfang Chen during the campaign and preparation of the manuscript.

References

Aiken, A. C., Decarlo, P. F., Kroll, J. H., Worsnop, D. R., Huffman, J. A., Docherty, K. S., Ulbrich, I. M., Mohr, C., Kimmel, J. R., Sueper, D., Sun, Y., Zhang, Q., Trimborn, A., Northway, M., Ziemann, P. J., Canagaratna, M. R., Onasch, T. B., Alfarra, M. R., Prevot, A. S. H., Dommen, J., Duplissy, J., Metzger, A., Baltensperger, U., and Jimenez, J. L.: O/C and OM/OC ratios of primary, secondary, and ambient organic aerosols with high-resolution time-of-flight aerosol mass spectrometry, Environ. Sci. Technol., 42, 4478-4485, 10.1021/Es703009q, 2008.

Aiken, A. C., de Foy, B., Wiedinmyer, C., DeCarlo, P. F., Ulbrich, I. M., Wehrli, M. N., Szidat, S., Prevot, A. S. H., Noda, J., Wacker, L., Volkamer, R., Fortner, E., Wang, J., Laskin, A., Shutthanandan, V., Zheng, J., Zhang, R., Paredes-Miranda, G., Arnott, W. P., Molina, L. T., Sosa, G., Querol, X., and Jimenez, J. L.: Mexico city aerosol analysis during MILAGRO using high resolution aerosol mass spectrometry at the urban supersite (T0) - Part 2: Analysis of the biomass burning contribution and the non-fossil carbon fraction, Atmos. Chem. Phys., 10, 5315-5341, 10.5194/acp-10-5315-2010, 2010.

Blando, J. D., and Turpin, B. J.: Secondary organic aerosol formation in cloud and fog droplets: a

615 literature evaluation of plausibility, Atmos. Environ., 34, 1623-1632, 10.1016/s1352-2310(99)00392-1,
616 2000.

617 Bozzetti, C., El Haddad, I., Salameh, D., Daellenbach, K. R., Fermo, P., Gonzalez, R., Minguillón, M.
618 C., Iinuma, Y., Poulain, L., Elser, M., Müller, E., Slowik, J. G., Jaffrezo, J. L., Baltensperger, U.,
619 Marchand, N., and Prévôt, A. S. H.: Organic aerosol source apportionment by offline-AMS over a full
620 year in Marseille, Atmos. Chem. Phys., 17, 8247-8268, 10.5194/acp-17-8247-2017, 2017.

621 Canagaratna, M. R., Jayne, J. T., Jimenez, J. L., Allan, J. D., Alfarra, M. R., Zhang, Q., Onasch, T. B.,
622 Drewnick, F., Coe, H., Middlebrook, A., Delia, A., Williams, L. R., Trimborn, A. M., Northway, M. J.,
623 DeCarlo, P. F., Kolb, C. E., Davidovits, P., and Worsnop, D. R.: Chemical and microphysical
624 characterization of ambient aerosols with the aerodyne aerosol mass spectrometer, Mass Spectrom.
625 Rev., 26, 185-222, 10.1002/Mas.20115, 2007.

626 Canagaratna, M. R., Jimenez, J. L., Kroll, J. H., Chen, Q., Kessler, S. H., Massoli, P., Hildebrandt Ruiz,
627 L., Fortner, E., Williams, L. R., Wilson, K. R., Surratt, J. D., Donahue, N. M., Jayne, J. T., and Worsnop,
628 D. R.: Elemental ratio measurements of organic compounds using aerosol mass spectrometry:
629 characterization, improved calibration, and implications, Atmos. Chem. Phys., 15, 253-272,
630 10.5194/acp-15-253-2015, 2015.

631 Carlton, A. G., Turpin, B. J., Lim, H. J., Altieri, K. E., and Seitzinger, S.: Link between isoprene and
632 secondary organic aerosol (SOA): Pyruvic acid oxidation yields low volatility organic acids in clouds,
633 Geophys. Res. Lett., 33, 10.1029/2005gl025374, 2006.

634 Carslaw, K. S., Boucher, O., Spracklen, D. V., Mann, G. W., Rae, J. G. L., Woodward, S., and Kulmala,
635 M.: A review of natural aerosol interactions and feedbacks within the Earth system, Atmos. Chem.
636 Phys., 10, 1701-1737, 10.5194/acp-10-1701-2010, 2010.

637 Chan, C. K., and Yao, X.: Air pollution in mega cities in China, Atmos. Environ., 42, 1-42,
638 10.1016/j.atmosenv.2007.09.003, 2008.

639 Cheng, Y., Zheng, G., Wei, C., Mu, Q., Zheng, B., Wang, Z., Gao, M., Zhang, Q., He, K., Carmichael,
640 G., Pöschl, U., and Su, H.: Reactive nitrogen chemistry in aerosol water as a source of sulfate during
641 haze events in China, Sci. Adv., 2, e1601530, 10.1126/sciadv.1601530, 2016.

642 Chhabra, P. S., Ng, N. L., Canagaratna, M. R., Corrigan, A. L., Russell, L. M., Worsnop, D. R., Flagan,
643 R. C., and Seinfeld, J. H.: Elemental composition and oxidation of chamber organic aerosol, Atmos.
644 Chem. Phys., 11, 8827-8845, 10.5194/acp-11-8827-2011, 2011.

645 De Haan, D. O., Hawkins, L. N., Kononenko, J. A., Turley, J. J., Corrigan, A. L., Tolbert, M. A., and
646 Jimenez, J. L.: Formation of nitrogen-nontaining oligomers by methylglyoxal and amines in simulated
647 evaporating cloud droplets, Environ. Sci. Technol., 45, 984-991, 10.1021/es102933x, 2011.

648 El Haddad, I., D'Anna, B., Temime-Roussel, B., Nicolas, M., Boreave, A., Favez, O., Voisin, D., Sciare,
649 J., George, C., Jaffrezo, J. L., Wortham, H., and Marchand, N.: Towards a better understanding of the
650 origins, chemical composition and aging of oxygenated organic aerosols: case study of a Mediterranean
651 industrialized environment, Marseille, Atmos. Chem. Phys., 13, 7875-7894, 10.5194/acp-13-7875-2013,

652 2013.

653 Ervens, B., Turpin, B. J., and Weber, R. J.: Secondary organic aerosol formation in cloud droplets and
654 aqueous particles (aqSOA): a review of laboratory, field and model studies, Atmos. Chem. Phys., 11,
655 11069-11102, 10.5194/acp-11-11069-2011, 2011.

656 Ervens, B.: Modeling the processing of aerosol and trace gases in clouds and fogs, Chem. Rev., 115,
657 4157-4198, 10.1021/cr5005887, 2015.

658 Ge, X., Wexler, A. S., and Clegg, S. L.: Atmospheric amines - Part II. Thermodynamic properties and
659 gas/particle partitioning, Atmos. Environ., 45, 561-577, 10.1016/j.atmosenv.2010.10.013, 2011a.

660 Ge, X., Wexler, A. S., and Clegg, S. L.: Atmospheric amines - Part I. A review, Atmos. Environ., 45,
661 524-546, 10.1016/j.atmosenv.2010.10.012, 2011b.

662 Ge, X., Zhang, Q., Sun, Y., Ruehl, C. R., and Setyan, A.: Effect of aqueous-phase processing on aerosol
663 chemistry and size distributions in Fresno, California, during wintertime, Environ. Chem., 9, 221-235,
664 10.1071/EN11168, 2012.

665 Ge, X., He, Y., Sun, Y., Xu, J., Wang, J., Shen, Y., and Chen, M.: Characteristics and formation
666 mechanisms of fine particulate nitrate in typical urban areas in China, Atmosphere, 8, 62, 2017a.

667 Ge, X., Li, L., Chen, Y., Chen, H., Wu, D., Wang, J., Xie, X., Ge, S., Ye, Z., Xu, J., and Chen, M.:
668 Aerosol characteristics and sources in Yangzhou, China resolved by offline aerosol mass spectrometry
669 and other techniques, Environ. Pollut., 225, 74-85, 10.1016/j.envpol.2017.03.044, 2017b.

670 George, C., Ammann, M., D'Anna, B., Donaldson, D. J., and Nizkorodov, S. A.: Heterogeneous
671 photochemistry in the atmosphere, Chem. Rev., 115, 4218-4258, 10.1021/cr500648z, 2015a.

672 George, K. M., Ruthenburg, T. C., Smith, J., Yu, L., Zhang, Q., Anastasio, C., and Dillner, A. M.: FT-IR
673 quantification of the carbonyl functional group in aqueous-phase secondary organic aerosol from
674 phenols, Atmos. Environ., 100, 230-237, 10.1016/j.atmosenv.2014.11.011, 2015b.

675 Gilardoni, S., Massoli, P., Paglione, M., Giulianelli, L., Carbone, C., Rinaldi, M., Decesari, S., Sandrini,
676 S., Costabile, F., Gobbi, G. P., Pietrogrande, M. C., Visentin, M., Scotto, F., Fuzzi, S., and Facchini, M.
677 C.: Direct observation of aqueous secondary organic aerosol from biomass-burning emissions, P. Natl.
678 Aacd. Sci. USA, 10.1073/pnas.1602212113, 2016.

679 Guo, H., Weber, R. J., and Nenes, A.: High levels of ammonia do not raise fine particle pH sufficiently
680 to yield nitrogen oxide-dominated sulfate production, Sci. Rep., 7, 12109,
681 10.1038/s41598-017-11704-0, 2017.

682 Hallquist, M., Wenger, J. C., Baltensperger, U., Rudich, Y., Simpson, D., Claeys, M., Dommen, J.,
683 Donahue, N. M., George, C., Goldstein, A. H., Hamilton, J. F., Herrmann, H., Hoffmann, T., Iinuma, Y.,
684 Jang, M., Jenkin, M. E., Jimenez, J. L., Kiendler-Scharr, A., Maenhaut, W., McFiggans, G., Mentel, T.
685 F., Monod, A., Prévôt, A. S. H., Seinfeld, J. H., Surratt, J. D., Szmigielski, R., and Wildt, J.: The
686 formation, properties and impact of secondary organic aerosol: current and emerging issues, Atmos.

687 Chem. Phys., 9, 5155-5236, 10.5194/acp-9-5155-2009, 2009.

688 Heal, M. R., Kumar, P., and Harrison, R. M.: Particles, air quality, policy and health, Chem. Soc. Rev.,
689 41, 6606-6630, 2012.

690 Heald, C. L., Jacob, D. J., Park, R. J., Russell, L. M., Huebert, B. J., Seinfeld, J. H., Liao, H., and
691 Weber, R. J.: A large organic aerosol source in the free troposphere missing from current models,
692 Geophys. Res. Lett., 32, L18809, 10.1029/2005GL023831, 2005.

693 Heald, C. L., Kroll, J. H., Jimenez, J. L., Docherty, K. S., DeCarlo, P. F., Aiken, A. C., Chen, Q., Martin,
694 S. T., Farmer, D. K., and Artaxo, P.: A simplified description of the evolution of organic aerosol
695 composition in the atmosphere, Geophys. Res. Lett., 37, L08803, 10.1029/2010gl042737, 2010.

696 Heringa, M. F., DeCarlo, P. F., Chirico, R., Tritscher, T., Clairotte, M., Mohr, C., Crippa, M., Slowik, J.
697 G., Pfaffenberger, L., Dommen, J., Weingartner, E., Prévôt, A. S. H., and Baltensperger, U.: A new
698 method to discriminate secondary organic aerosols from different sources using high-resolution aerosol
699 mass spectra, Atmos. Chem. Phys., 12, 2189-2203, 10.5194/acp-12-2189-2012, 2012.

700 Herndon, S. C., Onasch, T. B., Wood, E. C., Kroll, J. H., Canagaratna, M. R., Jayne, J. T., Zavala, M. A.,
701 Knighton, W. B., Mazzoleni, C., Dubey, M. K., Ulbrich, I. M., Jimenez, J. L., Seila, R., de Gouw, J. A.,
702 de Foy, B., Fast, J., Molina, L. T., Kolb, C. E., and Worsnop, D. R.: Correlation of secondary organic
703 aerosol with odd oxygen in Mexico City, Geophys. Res. Lett., 35, L15804, 10.1029/2008gl034058,
704 2008.

705 Herrmann, H., Schaefer, T., Tilgner, A., Styler, S. A., Weller, C., Teich, M., and Otto, T.: Tropospheric
706 aqueous-phase chemistry: Kinetics, mechanisms, and its coupling to a changing gas phase, Chem. Rev.,
707 115, 4259-4334, 10.1021/cr500447k, 2015.

708 Hu, J., Wang, Y., Ying, Q., and Zhang, H.: Spatial and temporal variability of PM2.5 and PM10 over
709 the North China Plain and the Yangtze River Delta, China, Atmos. Environ., 95, 598-609,
710 10.1016/j.atmosenv.2014.07.019, 2014.

711 Hu, J., Huang, L., Chen, M., Liao, H., Zhang, H., Wang, S., Zhang, Q., and Ying, Q.: Premature
712 mortality attributable to particulate matter in China: Source contributions and responses to reductions,
713 Environ. Sci. Technol., 51, 9950-9959, 10.1021/acs.est.7b03193, 2017.

714 Huang, R., Zhang, Y., Bozzetti, C., Ho, K., Cao, J., Han, Y., Daellenbach, K. R., Slowik, J. G., Platt, S.
715 M., Canonaco, F., Zotter, P., Wolf, R., Pieber, S. M., Bruns, E. A., Crippa, M., Ciarelli, G., Piazzalunga,
716 A., Schwikowski, M., Abbaszade, G., Schnelle-Kreis, J., Zimmermann, R., An, Z., Szidat, S.,
717 Baltensperger, U., Haddad, I. E., and Prevot, A. S. H.: High secondary aerosol contribution to
718 particulate pollution during haze events in China, Nature, 514, 218-222, 10.1038/nature13774, 2014.

719 Jimenez, J. L., Canagaratna, M. R., Donahue, N. M., Prevot, A. S. H., Zhang, Q., Kroll, J. H., DeCarlo,
720 P. F., Allan, J. D., Coe, H., Ng, N. L., Aiken, A. C., Docherty, K. S., Ulbrich, I. M., Grieshop, A. P.,
721 Robinson, A. L., Duplissy, J., Smith, J. D., Wilson, K. R., Lanz, V. A., Hueglin, C., Sun, Y. L., Tian, J.,
722 Laaksonen, A., Raatikainen, T., Rautiainen, J., Vaattovaara, P., Ehn, M., Kulmala, M., Tomlinson, J. M.,
723 Collins, D. R., Cubison, M. J., Dunlea, E. J., Huffman, J. A., Onasch, T. B., Alfarra, M. R., Williams, P.

724 I., Bower, K., Kondo, Y., Schneider, J., Drewnick, F., Borrmann, S., Weimer, S., Demerjian, K.,
725 Salcedo, D., Cottrell, L., Griffin, R., Takami, A., Miyoshi, T., Hatakeyama, S., Shimono, A., Sun, J. Y.,
726 Zhang, Y. M., Dzepina, K., Kimmel, J. R., Sueper, D., Jayne, J. T., Herndon, S. C., Trimborn, A. M.,
727 Williams, L. R., Wood, E. C., Middlebrook, A. M., Kolb, C. E., Baltensperger, U., and Worsnop, D. R.:
728 Evolution of organic aerosols in the atmosphere, Science, 326, 1525-1529, 10.1126/science.1180353,
729 2009.

730 Kerminen, V.-M., and Wexler, A. S.: Growth laws for atmospheric aerosol particles: An examination of
731 the bimodality of the accumulation mode, Atmos. Environ., 29, 3263-3275,
732 10.1016/1352-2310(95)00249-X, 1995.

733 Li, K., Chen, L., White, S. J., Zheng, X., Lv, B., Lin, C., Bao, Z., Wu, X., Gao, X., Ying, F., Shen, J.,
734 Azzi, M., and Cen, K.: Chemical characteristics and sources of PM1 during the 2016 summer in
735 Hangzhou, Environ. Pollut., 232, 42-54, 10.1016/j.envpol.2017.09.016, 2018.

736 Li, Y., Sun, Y., Zhang, Q., Li, X., Li, M., Zhou, Z., and Chan, C. K.: Real-time chemical
737 characterization of atmospheric particulate matter in China: A review, Atmos. Environ., 158, 270-304,
738 10.1016/j.atmosenv.2017.02.027, 2017.

739 Li, Y. J., Lee, B. Y. L., Yu, J. Z., Ng, N. L., and Chan, C. K.: Evaluating the degree of oxygenation of
740 organic aerosol during foggy and hazy days in Hong Kong using high-resolution time-of-flight aerosol
741 mass spectrometry (HR-ToF-AMS), Atmos. Chem. Phys., 13, 8739-8753, 10.5194/acp-13-8739-2013,
742 2013.

743 Lim, Y. B., Tan, Y., Perri, M. J., Seitzinger, S. P., and Turpin, B. J.: Aqueous chemistry and its role in
744 secondary organic aerosol (SOA) formation, Atmos. Chem. Phys., 10, 10521-10539,
745 10.5194/acp-10-10521-2010, 2010.

746 Lim, Y. B., Tan, Y., and Turpin, B. J.: Chemical insights, explicit chemistry, and yields of secondary
747 organic aerosol from OH radical oxidation of methylglyoxal and glyoxal in the aqueous phase, Atmos.
748 Chem. Phys., 13, 8651-8667, 10.5194/acp-13-8651-2013, 2013.

749 Lin, C., Ceburnis, D., Hellebust, S., Buckley, P., Wenger, J., Canonaco, F., Prévôt, A. S. H., Huang, R.,
750 O'Dowd, C., and Ovadnevaite, J.: Characterization of Primary Organic Aerosol from Domestic Wood,
751 Peat, and Coal Burning in Ireland, Environ. Sci. Technol., 51, 10624-10632, 10.1021/acs.est.7b01926,
752 2017.

753 Liu, M., Song, Y., Zhou, T., Xu, Z., Yan, C., Zheng, M., Wu, Z., Hu, M., Wu, Y., and Zhu, T.: Fine
754 particle pH during severe haze episodes in northern China, Geophys. Res. Lett., 44, 5213–5221,
755 10.1002/2017GL073210, 2017.

756 Liu, Y., Monod, A., Tritscher, T., Praplan, A. P., DeCarlo, P. F., Temime-Roussel, B., Quivet, E.,
757 Marchand, N., Dommen, J., and Baltensperger, U.: Aqueous phase processing of secondary organic
758 aerosol from isoprene photooxidation, Atmos. Chem. Phys., 12, 5879-5895, 10.5194/acp-12-5879-2012,
759 2012.

760 McNeill, V. F.: Aqueous organic chemistry in the atmosphere: Sources and chemical processing of

761 organic aerosols, Environ. Sci. Technol., 49, 1237-1244, 10.1021/es5043707, 2015.

762 Meng, Z., and Seinfeld, J. H.: On the source of the submicrometer droplet mode of urban and regional
763 aerosols, Aerosol Sci. Tech., 20, 253-265, 10.1080/02786829408959681, 1994.

764 Middlebrook, A. M., Bahreini, R., Jimenez, J. L., and Canagaratna, M. R.: Evaluation of
765 composition-dependent collection efficiencies for the Aerodyne aerosol mass spectrometer using field
766 data, Aerosol Sci. Tech., 46, 258-271, 10.1080/02786826.2011.620041, 2012.

767 Ng, N. L., Canagaratna, M. R., Zhang, Q., Jimenez, J. L., Tian, J., Ulbrich, I. M., Kroll, J. H., Docherty,
768 K. S., Chhabra, P. S., Bahreini, R., Murphy, S. M., Seinfeld, J. H., Hildebrandt, L., Donahue, N. M.,
769 DeCarlo, P. F., Lanz, V. A., Prevot, A. S. H., Dinar, E., Rudich, Y., and Worsnop, D. R.: Organic aerosol
770 components observed in Northern Hemispheric datasets from Aerosol Mass Spectrometry, Atmos.
771 Chem. Phys., 10, 4625-4641, 10.5194/acp-10-4625-2010, 2010.

772 Onasch, T. B., Trimborn, A., Fortner, E. C., Jayne, J. T., Kok, G. L., Williams, L. R., Davidovits, P., and
773 Worsnop, D. R.: Soot particle aerosol mass spectrometer: Development, validation, and initial
774 application, Aerosol Sci. Tech., 46, 804-817, 10.1080/02786826.2012.663948, 2012.

775 Pöschl, U.: Atmospheric aerosols: Composition, transformation, climate and health effects, Angew.
776 Chem., Int. Ed., 44, 7520-7540, 10.1002/anie.200501122, 2005.

777 Paatero, P., and Tapper, U.: Positive matrix factorization: A non-negative factor model with optimal
778 utilization of error estimates of data values, Environmetrics, 5, 111-126, 10.1002/env.3170050203,
779 1994.

780 Philip, S., Martin, R. V., Pierce, J. R., Jimenez, J. L., Zhang, Q., Canagaratna, M. R., Spracklen, D. V.,
781 Nowlan, C. R., Lamsal, L. N., Cooper, M. J., and Krotkov, N. A.: Spatially and seasonally resolved
782 estimate of the ratio of organic mass to organic carbon, Atmos. Environ., 87, 34-40,
783 10.1016/j.atmosenv.2013.11.065, 2014.

784 Pope, C. A., and Dockery, D. W.: Health effects of fine particulate air pollution: Lines that connect, J.
785 Air Waste Manage., 56, 709-742, 10.1080/10473289.2006.10464485, 2006.

786 Saffari, A., Hasheminassab, S., Shafer, M. M., Schauer, J. J., Chatila, T. A., and Sioutas, C.: Nighttime
787 aqueous-phase secondary organic aerosols in Los Angeles and its implication for fine particulate matter
788 composition and oxidative potential, Atmos. Environ., 133, 112-122, 10.1016/j.atmosenv.2016.03.022,
789 2016.

790 Seinfeld, J. H., and Pandis, S. N.: Atmospheric chemistry and physics: From air pollution to climate
791 change, John Wiley & Sons, New York, 2016.

792 Shen, F., Ge, X., Hu, J., Nie, D., Tian, L., and Chen, M.: Air pollution characteristics and health risks in
793 Henan Province, China, Environ. Res., 156, 625-634, 10.1016/j.envres.2017.04.026, 2017.

794 Shen, G., Xue, M., Yuan, S., Zhang, J., Zhao, Q., Li, B., Wu, H., and Ding, A.: Chemical compositions
795 and reconstructed light extinction coefficients of particulate matter in a mega-city in the western

796 Yangtze River Delta, China, Atmos. Environ., 83, 14-20, 10.1016/j.atmosenv.2013.10.055, 2014.

797 Shen, X. J., Sun, J. Y., Zhang, X. Y., Zhang, Y. M., Zhang, L., Che, H. C., Ma, Q. L., Yu, X. M., Yue, Y.,
798 and Zhang, Y. W.: Characterization of submicron aerosols and effect on visibility during a severe
799 haze-fog episode in Yangtze River Delta, China, Atmos. Environ., 120, 307-316,
800 10.1016/j.atmosenv.2015.09.011, 2015.

801 Shiraiwa, M., Ueda, K., Pozzer, A., Lammel, G., Kampf, C. J., Fushimi, A., Enami, S., Arangio, A. M.,
802 Fröhlich-Nowoisky, J., Fujitani, Y., Furuyama, A., Lakey, P. S. J., Lelieveld, J., Lucas, K., Morino, Y.,
803 Pöschl, U., Takahama, S., Takami, A., Tong, H., Weber, B., Yoshino, A., and Sato, K.: Aerosol health
804 effects from molecular to global scales, Environ. Sci. Technol., 51, 13545-13567,
805 10.1021/acs.est.7b04417, 2017.

806 Spracklen, D. V., Jimenez, J. L., Carslaw, K. S., Worsnop, D. R., Evans, M. J., Mann, G. W., Zhang, Q.,
807 Canagaratna, M. R., Allan, J., Coe, H., McFiggans, G., Rap, A., and Forster, P.: Aerosol mass
808 spectrometer constraint on the global secondary organic aerosol budget, Atmos. Chem. Phys., 11,
809 12109-12136, 10.5194/acp-11-12109-2011, 2011.

810 ToF-AMS Analysis Software, available at:
811 http://cires1.colorado.edu/jimenez-group/ToFAMSResources/ToFSoftware/index.html, 2015.

812 Sun, Y., Wang, Z., Fu, P., Jiang, Q., Yang, T., Li, J., and Ge, X.: The impact of relative humidity on
813 aerosol composition and evolution processes during wintertime in Beijing, China, Atmos. Environ., 77,
814 927-934, 10.1016/j.atmosenv.2013.06.019, 2013a.

815 Sun, Y., Du, W., Fu, P., Wang, Q., Li, J., Ge, X., Zhang, Q., Zhu, C., Ren, L., Xu, W., Zhao, J., Han, T.,
816 Worsnop, D. R., and Wang, Z.: Primary and secondary aerosols in Beijing in winter: sources, variations
817 and processes, Atmos. Chem. Phys., 16, 8309-8329, 10.5194/acp-16-8309-2016, 2016.

818 Sun, Y. L., Zhang, Q., Anastasio, C., and Sun, J.: Insights into secondary organic aerosol formed via
819 aqueous-phase reactions of phenolic compounds based on high resolution mass spectrometry, Atmos.
820 Chem. Phys., 10, 4809-4822, 10.5194/acp-10-4809-2010, 2010.

821 Sun, Y. L., Wang, Z. F., Fu, P. Q., Yang, T., Jiang, Q., Dong, H. B., Li, J., and Jia, J. J.: Aerosol
822 composition, sources and processes during wintertime in Beijing, China, Atmos. Chem. Phys., 13,
823 4577-4592, 10.5194/acp-13-4577-2013, 2013b.

824 Tie, X., Huang, R.-J., Cao, J., Zhang, Q., Cheng, Y., Su, H., Chang, D., Pöschl, U., Hoffmann, T.,
825 Dusek, U., Li, G., Worsnop, D. R., and O'Dowd, C. D.: Severe pollution in China amplified by
826 atmospheric moisture, Sci. Rep., 7, 15760, 10.1038/s41598-017-15909-1, 2017.

827 Ulbrich, I. M., Canagaratna, M. R., Zhang, Q., Worsnop, D. R., and Jimenez, J. L.: Interpretation of
828 organic components from Positive Matrix Factorization of aerosol mass spectrometric data, Atmos.
829 Chem. Phys., 9, 2891-2918, 10.5194/acp-9-2891-2009, 2009.

830 Wang, G., Zhang, R., Gomez, M. E., Yang, L., Levy Zamora, M., Hu, M., Lin, Y., Peng, J., Guo, S.,
831 Meng, J., Li, J., Cheng, C., Hu, T., Ren, Y., Wang, Y., Gao, J., Cao, J., An, Z., Zhou, W., Li, G., Wang,

J., Tian, P., Marrero-Ortiz, W., Secrest, J., Du, Z., Zheng, J., Shang, D., Zeng, L., Shao, M., Wang, W., Huang, Y., Wang, Y., Zhu, Y., Li, Y., Hu, J., Pan, B., Cai, L., Cheng, Y., Ji, Y., Zhang, F., Rosenfeld, D., Liss, P. S., Duce, R. A., Kolb, C. E., and Molina, M. J.: Persistent sulfate formation from London Fog to Chinese haze, P. Natl. Aacd. Sci. USA, 113, 13630-13635, 10.1073/pnas.1616540113, 2016a.

Wang, J., Ge, X., Chen, Y., Shen, Y., Zhang, Q., Sun, Y., Xu, J., Ge, S., Yu, H., and Chen, M.: Highly time-resolved urban aerosol characteristics during springtime in Yangtze River Delta, China: insights from soot particle aerosol mass spectrometry, Atmos. Chem. Phys., 16, 9109-9127, 10.5194/acp-16-9109-2016, 2016b.

Wang, J., Onasch, T. B., Ge, X., Collier, S., Zhang, Q., Sun, Y., Yu, H., Chen, M., Prévôt, A. S. H., and Worsnop, D. R.: Observation of fullerene soot in eastern China, Environ. Sci. Technol. Lett., 3, 121-126, 10.1021/acs.estlett.6b00044, 2016c.

Wang, X., Wang, W., Yang, L., Gao, X., Nie, W., Yu, Y., Xu, P., Zhou, Y., and Wang, Z.: The secondary formation of inorganic aerosols in the droplet mode through heterogeneous aqueous reactions under haze conditions, Atmos. Environ., 63, 68-76, 10.1016/j.atmosenv.2012.09.029, 2012.

Wexler, A. S., and Johnston, M. V.: What have we learned from highly time-resolved measurements during EPA's Supersites program,and related studies?, J. Air Waste Manage., 58, 303-319, 10.3155/1047-3289.58.2.303, 2008.

Wu, D., Zhang, F., Ge, X., Yang, M., Xia, J., Liu, G., and Li, F.: Chemical and light extinction characteristics of atmospheric aerosols in suburban Nanjing, China, Atmosphere, 8, 149, 10.3390/atmos8080149, 2017.

Xie, Y., Ding, A., Nie, W., Mao, H., Qi, X., Huang, X., Xu, Z., Kerminen, V.-M., Petäjä, T., Chi, X., Virkkula, A., Boy, M., Xue, L., Guo, J., Sun, J., Yang, X., Kulmala, M., and Fu, C.: Enhanced sulfate formation by nitrogen dioxide: Implications from in situ observations at the SORPES station, J. Geophys. Res., 120, 2015JD023607, 10.1002/2015JD023607, 2015.

Xu, W., Han, T., Du, W., Wang, Q., Chen, C., Zhao, J., Zhang, Y., Li, J., Fu, P., Wang, Z., Worsnop, D. R., and Sun, Y.: Effects of aqueous-phase and photochemical processing on secondary organic aerosol formation and evolution in Beijing, China, Environ. Sci. Technol., 51, 762-770, 10.1021/acs.est.6b04498, 2017a.

Xu, W., Sun, Y., Wang, Q., Du, W., Zhao, J., Ge, X., Han, T., Zhang, Y., Zhou, W., Li, J., Fu, P., Wang, Z., and Worsnop, D. R.: Seasonal characterization of organic nitrogen in atmospheric aerosols using high resolution aerosol mass spectrometry in Beijing, China, ACS Earth Space Chem., 1, 673-682, 10.1021/acsearthspacechem.7b00106, 2017b.

Yan, C., Zheng, M., Sullivan, A. P., Shen, G., Chen, Y., Wang, S., Zhao, B., Cai, S., Desyaterik, Y., Li, X., Zhou, T., Gustafsson, Ö., and Collett, J. L.: Residential coal combustion as a source of levoglucosan in China, Environ. Sci. Technol., 10.1021/acs.est.7b05858, 2018.

Yang, T., Sun, Y., Zhang, W., Wang, Z., Liu, X., Fu, P., and Wang, X.: Evolutionary processes and sources of high-nitrate haze episodes over Beijing, Spring, J. Environ. Sci., 54, 142-151,

10.1016/j.jes.2016.04.024, 2017.

Ye, Z., Li, Q., Liu, J., Luo, S., Zhou, Q., Bi, C., Ma, S., Chen, Y., Chen, H., Li, L., and Ge, X.: Investigation of submicron aerosol characteristics in Changzhou, China: Composition, source, and comparison with co-collected PM2.5, Chemosphere, 183, 176-185, https://doi.org/10.1016/j.chemosphere.2017.05.094, 2017a.

Ye, Z., Li, Q., Ma, S., Zhou, Q., Gu, Y., Su, Y., Chen, Y., Chen, H., Wang, J., and Ge, X.: Summertime day-night differences of PM2.5 components (inorganic ions, OC, EC, WSOC, WSON, HULIS, and PAHs) in Changzhou, China, Atmosphere, 8, 189, 10.3390/atmos8100189, 2017b.

Ye, Z., Liu, J., Gu, A., Feng, F., Liu, Y., Bi, C., Xu, J., Li, L., Chen, H., Chen, Y., Dai, L., Zhou, Q., and Ge, X.: Chemical characterization of fine particular matter in Changzhou, China and source apportionment with offline aerosol mass spectrometry, Atmos. Chem. Phys. , 2017, 2573-2592, 10.5194/acp-2016-883, 2017c.

Yu, L., Smith, J., Laskin, A., Anastasio, C., Laskin, J., and Zhang, Q.: Chemical characterization of SOA formed from aqueous-phase reactions of phenols with the triplet excited state of carbonyl and hydroxyl radical, Atmos. Chem. Phys., 14, 13801-13816, 10.5194/acp-14-13801-2014, 2014.

Yu, L., Smith, J., Laskin, A., George, K. M., Anastasio, C., Laskin, J., Dillner, A. M., and Zhang, Q.: Molecular transformations of phenolic SOA during photochemical aging in the aqueous phase: competition among oligomerization, functionalization, and fragmentation, Atmos. Chem. Phys., 16, 4511-4527, 10.5194/acp-16-4511-2016, 2016.

Zhang, C., Lu, X., Zhai, J., Chen, H., Yang, X., Zhang, Q., Zhao, Q., Fu, Q., Sha, F., and Jin, J.: Insights into the formation of secondary organic carbon in the summertime in urban Shanghai, J. Environ. Sci., 10.1016/j.jes.2017.12.018, 2018a.

Zhang, H., Chen, S., Zhong, J., Zhang, S., Zhang, Y., Zhang, X., Li, Z., and Zeng, X.: Formation of aqueous-phase sulfate during the haze period in China: Kinetics and atmospheric implications, Atmos. Environ., 10.1016/j.atmosenv.2018.01.017, 2018b.

Zhang, Q., Jimenez, J. L., Canagaratna, M. R., Allan, J. D., Coe, H., Ulbrich, I., Alfarra, M. R., Takami, A., Middlebrook, A. M., Sun, Y. L., Dzepina, K., Dunlea, E., Docherty, K., DeCarlo, P. F., Salcedo, D., Onasch, T., Jayne, J. T., Miyoshi, T., Shimono, A., Hatakeyama, S., Takegawa, N., Kondo, Y., Schneider, J., Drewnick, F., Borrmann, S., Weimer, S., Demerjian, K., Williams, P., Bower, K., Bahreini, R., Cottrell, L., Griffin, R. J., Rautiainen, J., Sun, J. Y., Zhang, Y. M., and Worsnop, D. R.: Ubiquity and dominance of oxygenated species in organic aerosols in anthropogenically-influenced Northern Hemisphere midlatitudes, Geophys. Res. Lett., 34, L13801, 10.1029/2007gl029979, 2007.

Zhang, Q., Jimenez, J., Canagaratna, M., Ulbrich, I., Ng, N., Worsnop, D., and Sun, Y.: Understanding atmospheric organic aerosols via factor analysis of aerosol mass spectrometry: a review, Anal. Bioanal. Chem., 401, 3045-3067, 10.1007/s00216-011-5355-y, 2011.

Zhang, R., Sun, X., Huang, Y., Shi, A., Yan, J., Nie, T., Yan, X., and Li, X.: Secondary inorganic aerosols formation during haze episodes at an urban site in Beijing, China, Atmos. Environ.,

906 10.1016/j.atmosenv.2017.12.031, 2018c.

907 Zhang, Y., Tang, L., Croteau, P. L., Favez, O., Sun, Y., Canagaratna, M. R., Wang, Z., Couvidat, F.,
908 Albinet, A., Zhang, H., Sciare, J., Prévôt, A. S. H., Jayne, J. T., and Worsnop, D. R.: Field
909 characterization of the PM2.5 Aerosol Chemical Speciation Monitor: insights into the composition,
910 sources, and processes of fine particles in eastern China, Atmos. Chem. Phys., 17, 14501-14517,
911 10.5194/acp-17-14501-2017, 2017.

912 Zhang, Y. J., Tang, L. L., Wang, Z., Yu, H. X., Sun, Y. L., Liu, D., Qin, W., Canonaco, F., Prévôt, A. S.
913 H., Zhang, H. L., and Zhou, H. C.: Insights into characteristics, sources, and evolution of submicron
914 aerosols during harvest seasons in the Yangtze River delta region, China, Atmos. Chem. Phys., 15,
915 1331-1349, 10.5194/acp-15-1331-2015, 2015a.

916 Zhang, Y. J., Tang, L., Yu, H., Wang, Z., Sun, Y., Qin, W., Chen, W., Chen, C., Ding, A., Wu, J., Ge, S.,
917 Chen, C., and Zhou, H.-c.: Chemical composition, sources and evolution processes of aerosol at an
918 urban site in Yangtze River Delta, China during wintertime, Atmos. Environ., 123, 339-349,
919 10.1016/j.atmosenv.2015.08.017, 2016.

920 Zhang, Y. W., Zhang, X. Y., Zhang, Y. M., Shen, X. J., Sun, J. Y., Ma, Q. L., Yu, X. M., Zhu, J. L.,
921 Zhang, L., and Che, H. C.: Significant concentration changes of chemical components of PM1 in the
922 Yangtze River Delta area of China and the implications for the formation mechanism of heavy
923 haze–fog pollution, Sci. Total Environ., 538, 7-15, 10.1016/j.scitotenv.2015.06.104, 2015b.

924

925

Atmos. Chem. Phys. Discuss., https://doi.org/10.5194/acp-2018-75
Manuscript under review for journal Atmos. Chem. Phys.
Discussion started: 5 February 2018

Atmospheric Chemistry and Physics Discussions

926

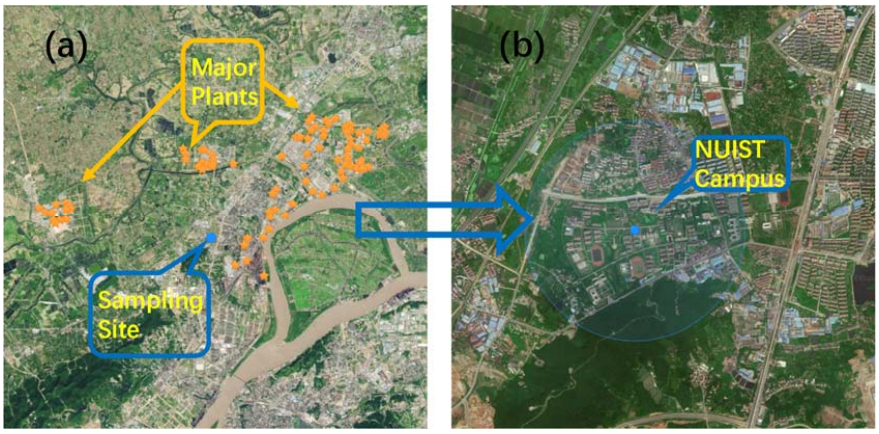

927

928 Figure 1. (a) The sampling site and its surroundings. The solid blue point is the
929 sampling site inside the campus of Nanjing University of Information Science and
930 Technology (NUIST) (b). The orange stars mark the positions of the major plants
931 adjacent to the site.

932

Atmos. Chem. Phys. Discuss., https://doi.org/10.5194/acp-2018-75
Manuscript under review for journal Atmos. Chem. Phys.
Discussion started: 5 February 2018

Atmospheric Chemistry and Physics Discussions

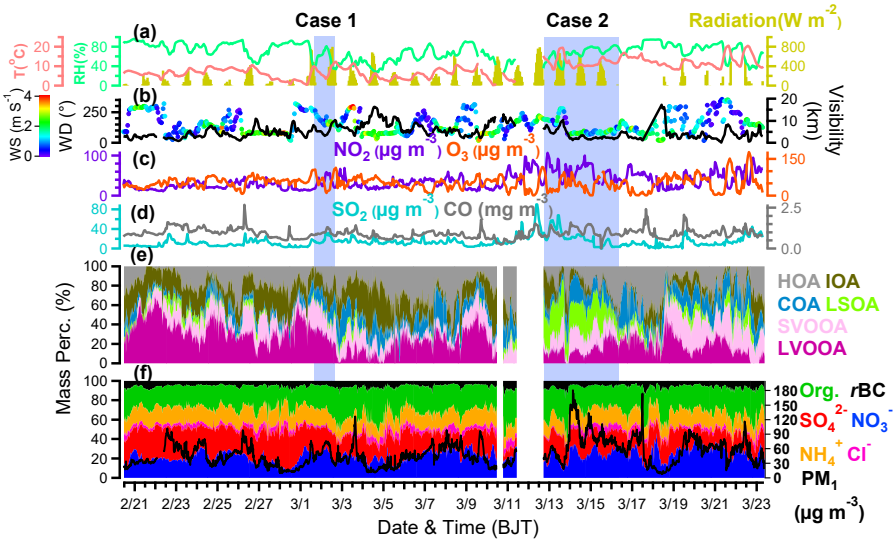

Figure 2. Time series of (a) air temperature (T), relative humidity (RH), and solar radiation; (b) wind direction (WD) colored by wind speed (WS), and visibility (km); (c-d) mass concentrations of NO_2, O_3, SO_2 and CO (hourly data); (e) mass contributions (%) of the OA subcomponents including the hydrocarbon-like organic aerosol (HOA), industry-related OA (IOA), cooking OA (COA), local secondary OA (LSOA), semi-volatile oxygenated OA (SVOOA) and low-volatility oxygenated OA (LVOOA); and (f) mass contributions (%) of refractory black carbon (*r*BC), total organics, ammonium, chloride, sulfate and nitrate. Two specific episodes are marked in light purple. (BJT, Beijing Time).

Atmos. Chem. Phys. Discuss., https://doi.org/10.5194/acp-2018-75
Manuscript under review for journal Atmos. Chem. Phys.
Discussion started: 5 February 2018

Atmospheric Chemistry and Physics Discussions

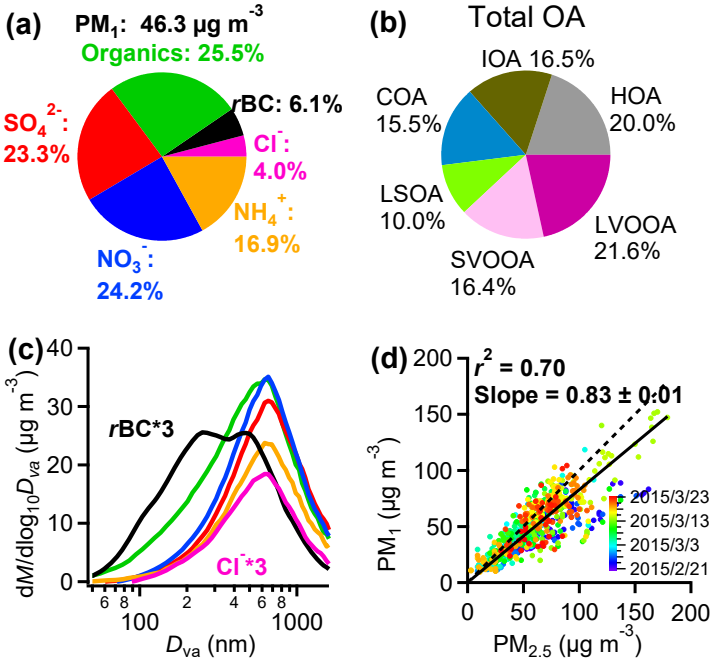

943

944 Figure 3. (a) Campaign-averaged mass fractions of *r*BC, organics, sulfate, nitrate,
945 ammonium and chloride to the total PM_1; (b) campaign-averaged mass fractions of
946 the six OA factors to the total OA; (c) mass-based campaign-average size distributions
947 of *r*BC (×3), organics, sulfate, nitrate, ammonium and chloride (×3); (d) scatter plots
948 of the PM_1 determined in this study *vs.* the $PM_{2.5}$ from government monitoring station
949 (colored by time).

950

Atmos. Chem. Phys. Discuss., https://doi.org/10.5194/acp-2018-75
Manuscript under review for journal Atmos. Chem. Phys.
Discussion started: 5 February 2018

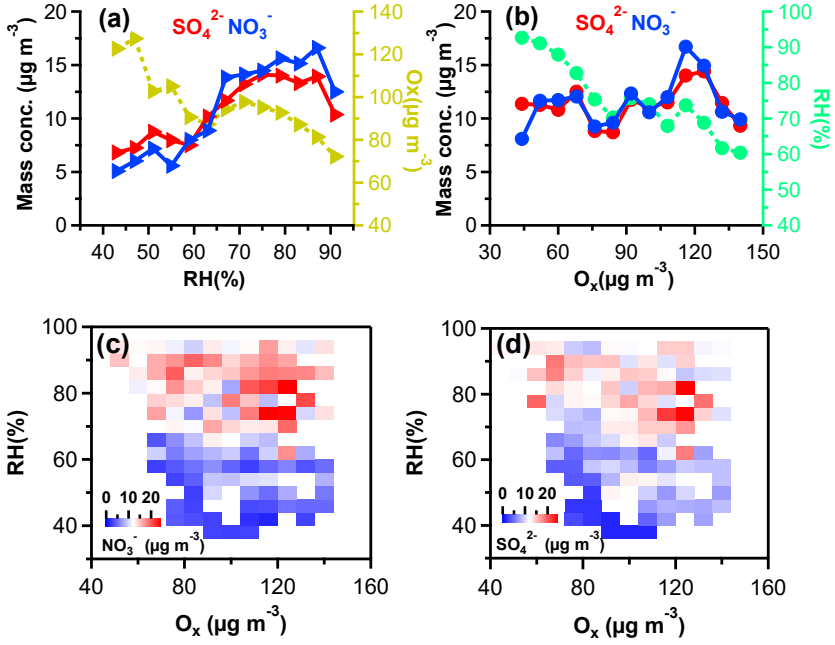

Figure 4. (a) Sulfate, nitrate and O_x concentrations *vs.* RH (5% increment); (b) sulfate, nitrate concentrations and RH *vs.* O_x concentrations (8 μg/m^3 increment); (c-d) RH-O_x image plots colored by sulfate and nitrate concentrations, respectively.

Atmos. Chem. Phys. Discuss., https://doi.org/10.5194/acp-2018-75
Manuscript under review for journal Atmos. Chem. Phys.
Discussion started: 5 February 2018

Atmospheric Chemistry and Physics Discussions

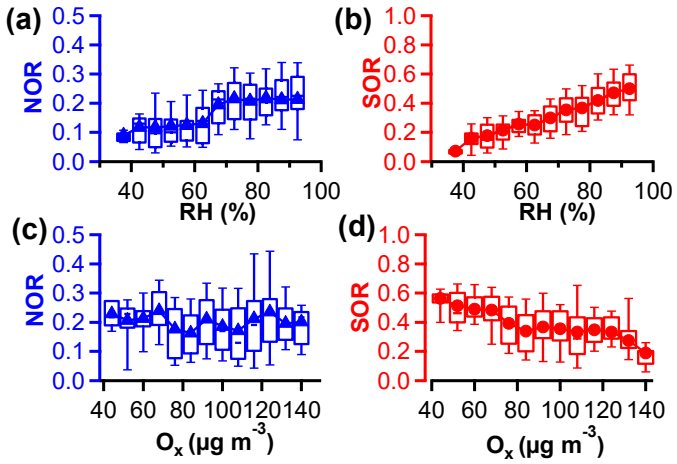

Figure 5. (a-b) Variations of nitrogen oxidation ratio (NOR)(a) and sulfur oxidation ratio (SOR) (b) as a function of RH (5% increment); and (c-d) NOR and SOR variations as a function of O_x concentrations (8 μg/m^3 increment) (the lines and solid triangles are the mean values, the lines in the boxes are the median values, the upper and lower boundaries of the boxes indicate the 75th and 25th percentiles, and the whiskers above and below the boxes indicate the 90th and 10th percentiles).

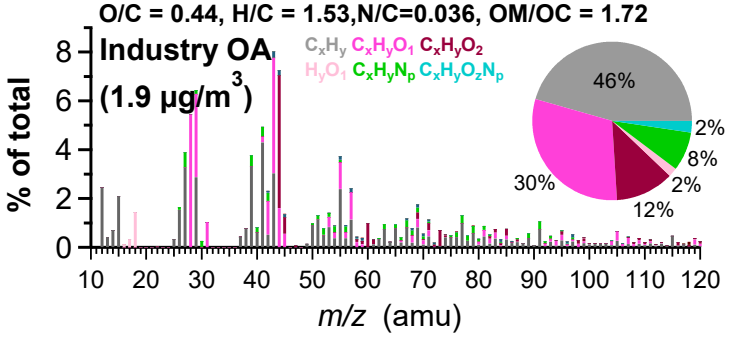

Figure 6. High-resolution mass spectrum of the industry-related OA (IOA) colored by six ion categories (the inset pie shows the relative mass contributions of the six ion categories).

Atmos. Chem. Phys. Discuss., https://doi.org/10.5194/acp-2018-75
Manuscript under review for journal Atmos. Chem. Phys.
Discussion started: 5 February 2018

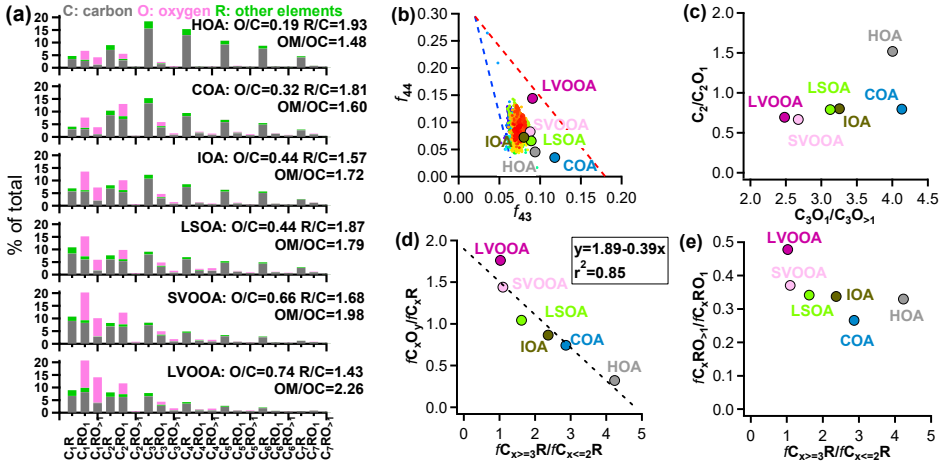

Figure 7. (a) Mass spectra of the six OA factors resorted by the ion groups with different carbon numbers (1-7) and oxygen numbers (0, 1, >1); (b) triangle plot of *f*44 *vs.* *f*43 for all OA (colored by time) and the six OA factors; and distributions of the six OA factors in the C_2/C_2O_1 *vs.* $C_3O_1/C_3O_{>1}$ space (c), the fC_xO_y/fC_xR *vs.* $fC_{x\geq3}R/fC_{x\leq2}R$ space (d), and the $fC_xRO_{>1}/fC_xRO_1$ *vs.* $fC_{x\geq3}R/fC_{x\leq2}R$ space (Meanings of the ion groups are described in the main text).

Atmos. Chem. Phys. Discuss., https://doi.org/10.5194/acp-2018-75
Manuscript under review for journal Atmos. Chem. Phys.
Discussion started: 5 February 2018

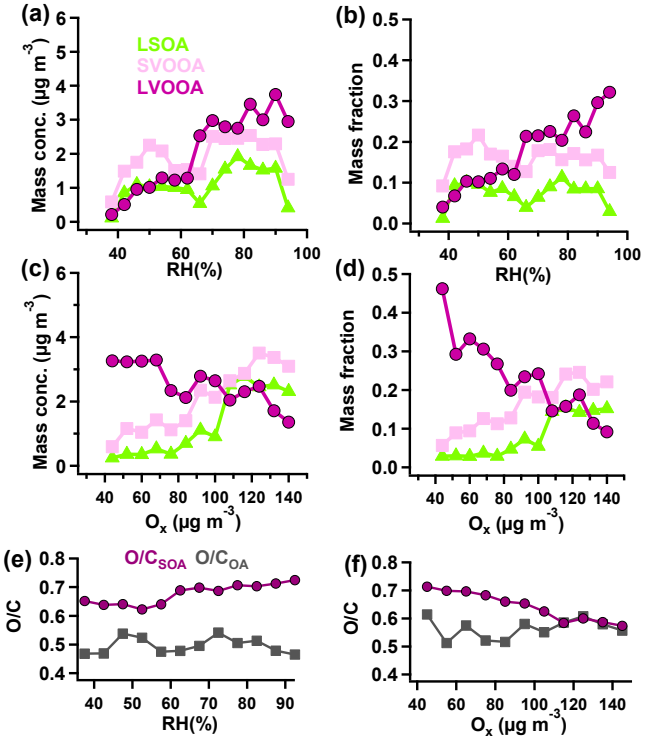

Figure 8. Mass concentrations (a) and fractional contributions (b) of the LSOA, SVOOA and LVOOA as a function of RH (5% increment); mass concentrations (c) and fractional contributions of LSOA, SVOOA and LVOOA as a function of O_x concentrations (8 μg/m^3 increment); and the O/C values of total OA (O/C_{OA}) and SOA (O/C_{SOA}) against RH (e) and O_x concentrations (f).

Atmos. Chem. Phys. Discuss., https://doi.org/10.5194/acp-2018-75
Manuscript under review for journal Atmos. Chem. Phys.
Discussion started: 5 February 2018

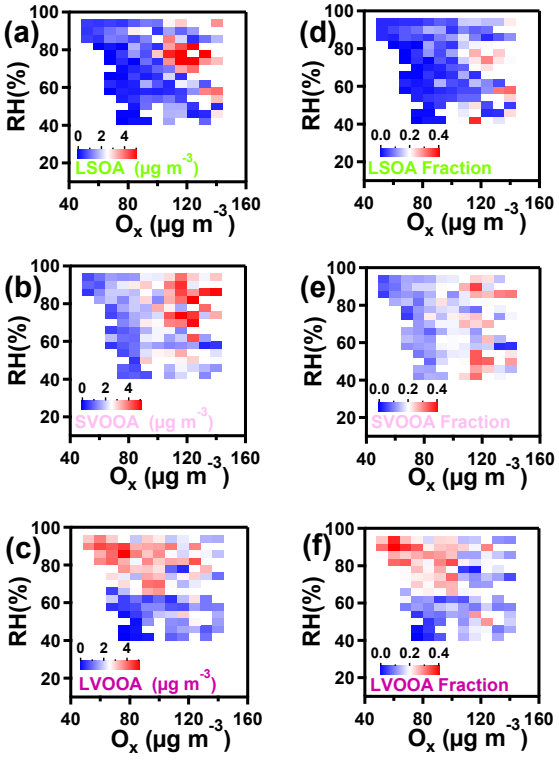

Figure 9. RH-O_x image plots colored by the mass concentrations of LSOA, SVOOA and LVOOA (a-c), and the mass fractions of LSOA, SVOOA and LVOOA to total OA (d-f).

Atmos. Chem. Phys. Discuss., https://doi.org/10.5194/acp-2018-75
Manuscript under review for journal Atmos. Chem. Phys.
Discussion started: 5 February 2018

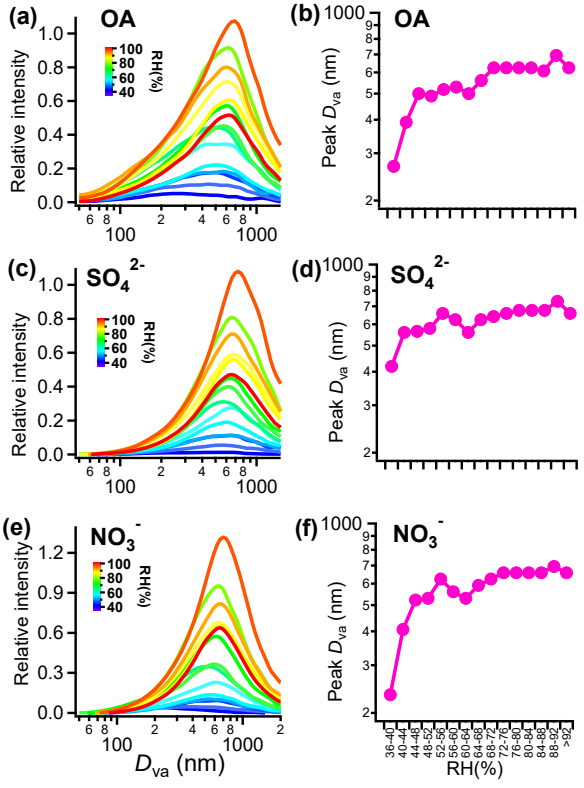

Figure 10. Average size distributions and the peak D_{va} of OA (a-b), sulfate (c-d) and nitrate (e-f) at different RH bins (4% increment).

Atmos. Chem. Phys. Discuss., https://doi.org/10.5194/acp-2018-75
Manuscript under review for journal Atmos. Chem. Phys.
Discussion started: 5 February 2018

Atmospheric Chemistry and Physics Discussions

993

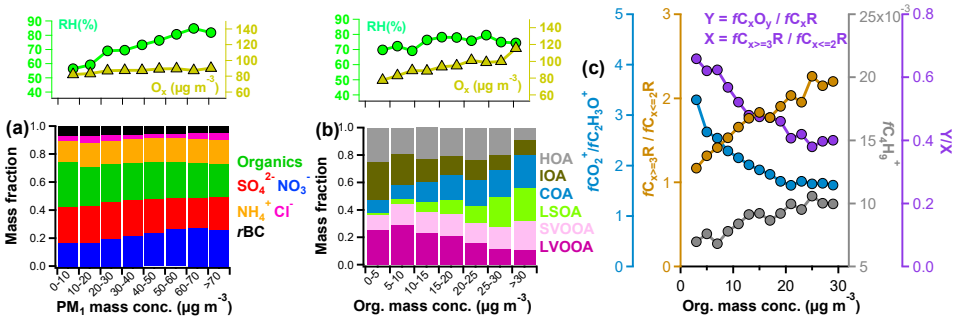

994

995 Figure 11. (a) Mass fractions of the six PM_1 components, and corresponding average
996 RH values and O_x concentrations at different PM_1 concentrations bins (10 μg/m^3
997 increment); (b) mass fractions of the six OA factors, and corresponding average RH
998 values and O_x concentrations at different OA concentration bins (5 μg/m^3 increment);
999 (c) $fCO_2^+/fC_2H_3O^+$, $fC_{x\geq3}R/fC_{x\leq2}R$, $fC_4H_9^+$ and $(fC_xO_y/fC_xR)/(fC_{x\geq3}R/fC_{x\leq2}R)$ as a
1000 function of OA concentrations.

1001

Atmos. Chem. Phys. Discuss., https://doi.org/10.5194/acp-2018-75
Manuscript under review for journal Atmos. Chem. Phys.
Discussion started: 5 February 2018

Atmospheric Chemistry and Physics Discussions

1002

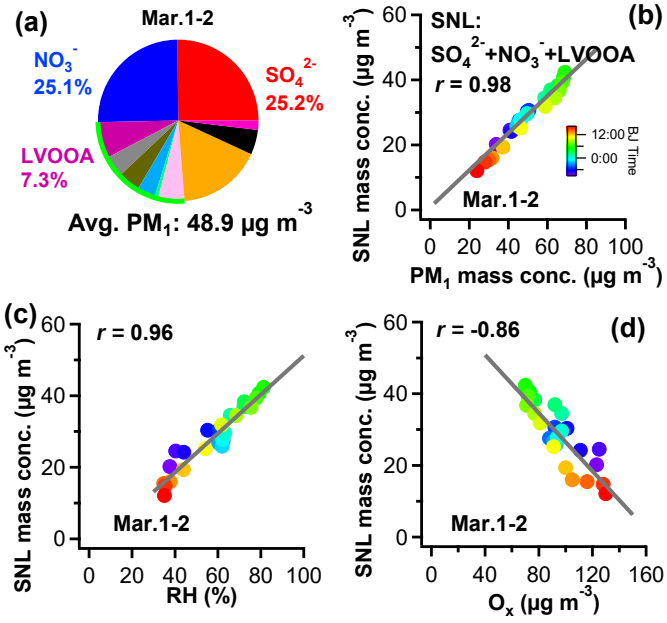

1003

1004 Figure 12. Case 1 (3:30 pm March 1 – 3:30 pm March 2): (a) average mass
1005 percentages of different species; scatter plots of SNL concentrations (the sum of
1006 sulfate, nitrate and LVOOA concentrations) *vs.* PM_1 concentrations (b), RH (c) and O_x
1007 concentrations (d) (colored by time).

1008

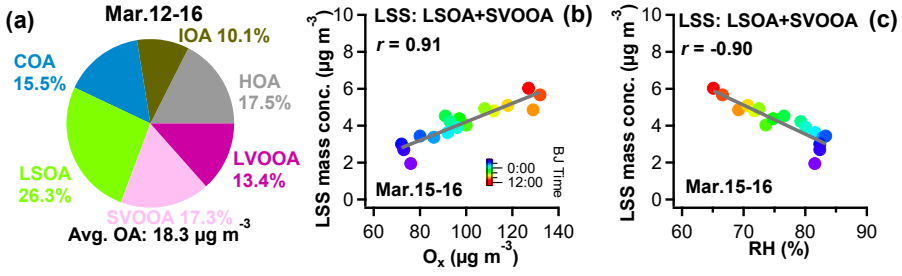

1009

1010 Figure 13. Case 2 (6:30 pm March 12 – 8:00 am March 16): (a) average mass
1011 contributions of the six OA factors to OA; scatter plots of LSS concentrations (the
1012 sum of LSOA and SVOOA concentrations) *vs.* O_x concentrations (b) and RH (c)
1013 (colored by time) (the data was only for 12:00 pm March 15 – 8:00 am March 16).

1014